J. Fluid Mech. (2013), *vol.* 718, *pp.* 181–209.
doi:10.1017/jfm.2012.604

Libration-induced mean flow in a spherical shell

Alban Sauret and Stéphane Le Dizès†

Institut de Recherche sur les Phénomènes Hors Équilibre, CNRS, and Aix-Marseille University, 49 rue F. Joliot-Curie, F-13013 Marseille, France

(Received 23 February 2012; revised 12 September 2012; accepted 3 December 2012)

We investigate the flow in a spherical shell subject to a time harmonic oscillation of its rotation rate, also called longitudinal libration, when the oscillation frequency is larger than twice the mean rotation rate. In this frequency regime, no inertial waves are directly excited by harmonic forcing. We show, however, that, through nonlinear interactions in the Ekman layers, it can generate a strong mean zonal flow in the interior. An analytical theory is developed using a perturbative approach in the limit of small libration amplitude ε and small Ekman number E. The mean flow is found to be at leading order an azimuthal flow that scales as the square of the libration amplitude and depends only on the cylindrical radius coordinate. The mean flow also exhibits a discontinuity across the cylinder tangent to the inner sphere. We show that this discontinuity can be smoothed through multi-scale Stewartson layers. The mean flow is also found to possess a weak axial flow that scales as $O(\varepsilon^2 E^{5/42})$ in the Stewartson layers. The analytical solution is compared to axisymmetric numerical simulations, and a good agreement is demonstrated.

Key words: boundary layers, geophysical and geological flows

1. Introduction

Most astrophysical bodies, in addition to their rotation, are subject to harmonic forcing such as precession, tidal deformation and latitudinal and longitudinal librations. The nonlinear corrections induced by such a forcing can lead to important steady and axisymmetric flow, called zonal flow, in the liquid core of telluric planets, in the subsurface ocean of some satellites or in the atmosphere of gaseous planets. In this study, we focus on longitudinal libration, which corresponds to a harmonic oscillation of the rotation rate. These oscillations are generally induced by gravitational coupling between an astrophysical body and its main gravitational partner around which it orbits (Comstock & Bills 2003). The librational forcing can have a non-negligible contribution in the internal dynamics of a planet, and a better knowledge of this dynamics can yield important information on the structure of a planet, such as an estimation of the thickness of the fluid layer under the ice shell in some satellites such as Europa, Ganymede or Encelade (Spohn & Schubert 2003; Lorenz *et al.* 2008; Van Hoolst *et al.* 2008; Rambaux, Van Hoolst & Karatekin 2011) or the existence of an inner liquid core in telluric planets such as Mercury (Margot *et al.* 2007).

† Email address for correspondence: ledizes@irphe.univ-mrs.fr

In the present work, we derive rigorous results for fast longitudinal libration when the libration frequency is at least twice as large as the spin frequency. Such a configuration is not the most common situation, as the main libration frequency often corresponds to the orbital frequency, which is generally equal to or smaller than the spin frequency. Here are a few situations that could exhibit fast libration. For example, one could imagine a planet or a satellite for which the spin and orbital frequencies are in resonance with a ratio $1:2$. This situation, which is in principle possible (Goldreich & Peale 1966; Wieczorek *et al.* 2012), would lead to fast libration with a libration frequency equal to twice the orbital frequency. Fast libration could also be present in a spin–orbit synchronized object when the forcing is induced by another satellite or planet with a larger orbital frequency. The Galilean satellites (Io, Europa and Ganymede) are in this situation. Io has an orbital frequency twice that of Europa, and four times as large as that of Ganymede. It could *a priori* then force the libration of Europa and of Ganymede with a frequency twice and four times as large as their spin frequency, respectively. A similar situation can also be found in exoplanetary systems. For instance, the two first planets in the 55 Cancri system have orbital frequencies of 2.81 and 14.65 days (Fischer, Marcy & Butler 2008). Since the two planets are expected to be spin–orbit synchronized, the frequency of libration of the second planet induced by the motion of the first planet would be $\omega = 14.65/2.81 \approx 5.2$.

The first analytical study of nonlinear effects generated by harmonic forcing was performed by Busse (1968) in the case of precession in a spheroid. He showed that a zonal flow is generated in the bulk as an effect of the nonlinear interactions in the viscous boundary layers. Wang (1970) studied theoretically and experimentally the nonlinear effects associated with an oscillation of the rotation rate in a cylindrical container (see also Busse 2010*b*). The case of a fixed tidal deformation was considered by Suess (1971), who argued that a counter-rotating vortex should exist near the axis of rotation. Aldridge & Toomre (1969) analysed librating spheres, but their experimental study focused on the linear response in the presence of inertial waves: they showed using pressure measurements that inertial waves can be resonantly excited in a librating sphere for particular libration frequencies. This has been confirmed numerically by Rieutord (1991). In his thesis, Aldridge (1967) also mentioned that, when the inertial waves are not significant, the flow in the bulk seems to drift, with an amplitude proportional to the square of the libration amplitude, but he did not report any quantitative measurement. Tilgner (1999) investigated numerically the linear response to the librational forcing in a spherical shell and studied the effect of the presence of an inner core, but he focused on the inertial waves and the attractors only. Recently, Calkins *et al.* (2010) studied numerically the mean zonal flow in the same geometry. They confirmed the presence of a mean zonal flow independent of the Ekman number and which scales as the square of the libration amplitude. However, their study remained mainly limited to a fixed frequency. Some laser Doppler velocimetry (LDV) measurements of the mean zonal flow have also been performed by Noir *et al.* (2010) in a cylindrical geometry. In this geometry, Sauret *et al.* (2012) analysed numerically the influence of the libration frequency. They found that the mean zonal flow was well described by the theory of Wang (1970) as long as no inertial waves are excited. The only theoretical study of the zonal flow in a spherical geometry is the recent work by Busse (2010*a*). He obtained by asymptotic methods an analytical prediction of the mean zonal flow in the limits of small libration frequencies and small Ekman numbers. The present paper extends this theory to the case of a spherical shell for any frequency.

The study implicitly assumes the absence of instability. Both shear and centrifugal instability are *a priori* possible when the amplitude of libration becomes sufficiently large. Centrifugal instability has been analysed in detail in a cylindrical geometry by Ern & Wesfreid (1999) and Sauret *et al.* (2012). It has also been observed in a librating sphere by Noir *et al.* (2009). Shear instability is present in planar Stokes layers (e.g. Davis 1976), but no clear evidence has been provided so far in cylindrical and spherical geometries. In the present study, the forcing amplitude is assumed to be sufficiently small that the flow generated at the libration frequency remains stable. To fully resolve this leading-order flow, we also assume that the libration frequency is larger than twice the mean rotation rate (spin frequency). This hypothesis guarantees that no inertial waves are excited and no critical latitude singularity is present. It will allow us to obtain an expression for the mean zonal flow in the whole shell. An expression for the mean zonal flow will also be provided for smaller frequencies (smaller than twice the mean rotation frequency) but it will exhibit a divergence associated with the presence of a critical latitude. We shall see that, for any libration frequency, the presence of an inner core significantly modifies the mean zonal flow and generates so-called Stewartson layers (Stewartson 1966) across the cylinder tangent to the inner core.

The paper is organized as follows. In § 2, we present the mathematical framework of the problem. We provide the governing equations and the hypothesis for the asymptotic analysis. The leading-order solution at the libration amplitude ε is derived in § 3. In § 4, we focus on the mean flow correction at the order ε^2. We explain how the nonlinear interactions within the Ekman layer generate a mean zonal flow in the bulk of the shell. We show that a discontinuity appears across the cylinder tangent to the inner core, which requires the introduction of viscous layers as for differentially rotating concentric spheres (Stewartson 1966). The structure of the solution in these layers is provided. We show that both axial vorticity and axial flow are the strongest in these layers. The details of the calculation leading to the expression of the different fields are given in the appendices. In § 5, the asymptotic solution is compared to numerical results obtained for both a sphere and a shell, and a fairly good agreement is obtained. A brief conclusion with some perspectives is provided in § 6.

2. Framework of the asymptotic analysis

We consider a homogeneous and incompressible fluid of kinematic viscosity ν contained in a spherical shell of external radius R_{ext} and inner radius R_{int}. This shell rotates in the laboratory frame at an angular velocity that oscillates sinusoidally around a mean angular value Ω_0. We use R_{ext} and ${\Omega_0}^{-1}$ as the length scale and the time scale, respectively. As both the libration forcing and the geometry are axisymmetric, we shall assume that the flow remains axisymmetric, that is, its velocity and pressure fields are independent of the azimuthal variable ϕ. It is then convenient to use the spherical coordinates (r, θ, ϕ) and to express the velocity field (u_r, u_θ, u_ϕ) as functions of ψ and χ defined by

$$u_r = \frac{1}{r^2 \sin\theta}\frac{\partial \psi}{\partial \theta}, \quad u_\theta = -\frac{1}{r \sin\theta}\frac{\partial \psi}{\partial r}, \quad u_\phi = \frac{\chi}{r \sin\theta}. \tag{2.1}$$

The use of a toroidal-poloidal decomposition of the velocity field is also possible (see e.g. Dormy & Jault 1998), but we prefer the formulation of Stewartson (1966) to use the similarity with his analysis.

In the frame rotating at the mean angular velocity, the dimensionless Navier–Stokes and continuity equations can be expressed as

$$\frac{\partial D^2\psi}{\partial t} - 2\left(\frac{\sin\theta}{r}\frac{\partial\chi}{\partial\theta} - \cos\theta\frac{\partial\chi}{\partial r}\right) - E\,D^4\psi = \frac{2\chi}{r^2\sin^2\theta}\left(\frac{\sin\theta}{r}\frac{\partial\chi}{\partial\theta} - \cos\theta\frac{\partial\chi}{\partial r}\right) + \frac{1}{r^2\sin\theta}\left(\frac{\partial\psi}{\partial r}\frac{\partial D^2\psi}{\partial\theta} - \frac{\partial\psi}{\partial\theta}\frac{\partial D^2\psi}{\partial r}\right) + \frac{2D^2\psi}{r^2\sin^2\theta}\left(\frac{\sin\theta}{r}\frac{\partial\psi}{\partial\theta} - \cos\theta\frac{\partial\psi}{\partial r}\right), \tag{2.2}$$

$$\frac{\partial\chi}{\partial t} + 2\left(\frac{\sin\theta}{r}\frac{\partial\psi}{\partial\theta} - \cos\theta\frac{\partial\psi}{\partial r}\right) - E\,D^2\chi = \frac{1}{r^2\sin\theta}\left(\frac{\partial\psi}{\partial r}\frac{\partial\chi}{\partial\theta} - \frac{\partial\psi}{\partial\theta}\frac{\partial\chi}{\partial r}\right), \tag{2.3}$$

where

$$D^2 = \frac{\partial^2}{\partial r^2} + \frac{\sin\theta}{r^2}\frac{\partial}{\partial\theta}\left(\frac{1}{\sin\theta}\frac{\partial}{\partial\theta}\right) \tag{2.4}$$

and E is the Ekman number defined by

$$E = \frac{\nu}{\Omega R_{ext}^2}. \tag{2.5}$$

We consider no-slip boundary conditions for a general configuration where the outer sphere and the inner core do not librate at the same amplitude. The boundary conditions in the rotating frame of reference then read for the functions ψ and χ:

$$\frac{\partial\psi}{\partial r} = \psi = 0 \quad \text{and} \quad \chi = \varepsilon\sin^2\theta\cos(\omega t) \quad \text{at } r = 1, \tag{2.6a}$$

$$\frac{\partial\psi}{\partial r} = \psi = 0 \quad \text{and} \quad \chi = \varepsilon\alpha a^2\sin^2\theta\cos(\omega t) \quad \text{at } r = a, \tag{2.6b}$$

where $a = R_{int}/R_{ext}$ is the aspect ratio of the shell, ε the amplitude of libration of the outer sphere and ω the frequency of libration. The parameter α measures the relative amplitude of libration of the inner core. For a non-librating inner core, we impose $\alpha = 0$; whereas, when it is librating at the same amplitude as the outer sphere, $\alpha = 1$. For the case of a sphere, without inner core, only the condition at $r = 1$ has to be applied.

The objective of our work is to characterize the steady flow induced by the librational forcing. We assume that the forcing amplitude ε is small such that the flow remains stable with respect to the centrifugal instability. Moreover, we consider the limit $\varepsilon \ll 1$ in order to use asymptotic methods. In this limit, we can expand the functions ψ and χ in powers of ε:

$$\psi = \varepsilon\psi_1 + \varepsilon^2\psi_2 + o(\varepsilon^2), \tag{2.7a}$$

$$\chi = \varepsilon\chi_1 + \varepsilon^2\chi_2 + o(\varepsilon^2). \tag{2.7b}$$

The first-order solution is expected to be the linear response at the librating frequency forced by the boundary, while the second-order solution represents that generated by the nonlinear interactions of the first-order solution with itself. As in all weakly nonlinear analysis, both harmonic corrections oscillating at 2ω and mean flow corrections (the zonal flow) are expected. It is this second part due to its peculiar structure that will be our point of focus.

3. Linear solution

In this section, we consider the solution obtained at the order ε. We are interested in the solution for very small values of E, as encountered in geophysical applications. For this reason, it is natural to consider E as an asymptotically small parameter. Nevertheless, this limit is taken after having considered $\varepsilon \to 0$. In the small E limit, we expect viscous effects to be localized in space. In our analysis, we shall require that, for the first-order solution, they are localized near the boundaries. This strong constraint can be satisfied if no inertial waves are excited in the bulk by the harmonic forcing. This is verified if the frequency of the forcing is outside the range of inertial wave frequencies, that is, $\omega > 2$, which is the condition that we shall assume in the following.

For $\omega > 2$, the linear response is expected to be mainly localized close to the boundaries. This solution can be obtained by performing a classical asymptotic analysis as done for Stokes or Ekman layers. Let us consider first the boundary layer on the outer sphere at $r = 1$. The boundary layer solution is obtained by introducing the local variable $\tilde{r} = (1 - r)/\sqrt{E}$. Let us write the leading-order expressions for ψ and χ as

$$\psi_1 \sim \sqrt{E}\,\psi_1^{(o)} \mathrm{e}^{\mathrm{i}\omega t} + \text{c.c.}, \tag{3.1a}$$

$$\chi_1 \sim \chi_1^{(o)} \mathrm{e}^{\mathrm{i}\omega t} + \text{c.c.}, \tag{3.1b}$$

where the superscript (o) indicates that we consider the function in the viscous layer at the boundary of the outer sphere and c.c. denotes complex conjugate. Inserting (2.7*a*) and (2.7*b*) with (3.1*a*) and (3.1*b*) into (2.2) and (2.3), we obtain, at leading order in E and ε, the equations

$$\mathrm{i}\omega \frac{\partial^2 \psi_1^{(o)}}{\partial \tilde{r}^2} - 2\cos\theta \frac{\partial \chi_1^{(o)}}{\partial \tilde{r}} = \frac{\partial^4 \psi_1^{(o)}}{\partial \tilde{r}^4}, \tag{3.2a}$$

$$\mathrm{i}\omega \chi_1^{(o)} + 2\cos\theta \frac{\partial \psi_1^{(o)}}{\partial \tilde{r}} = \frac{\partial^2 \chi_1^{(o)}}{\partial \tilde{r}^2}, \tag{3.2b}$$

with the no-slip boundary conditions

$$\psi_1^{(o)}(\tilde{r} = 0, \theta) = 0, \tag{3.3a}$$

$$\partial_{\tilde{r}} \psi_1^{(o)}(\tilde{r} = 0, \theta) = 0, \tag{3.3b}$$

$$\chi_1^{(o)}(\tilde{r} = 0, \theta) = (\sin^2\theta)/2. \tag{3.3c}$$

These equations, together with the boundary conditions, give

$$\psi_1^{(o)} = \frac{\mathrm{i}\sin^2\theta}{4}\left[\frac{1 - \mathrm{e}^{-\lambda_+ \tilde{r}}}{\lambda_+} - \frac{1 - \mathrm{e}^{-\lambda_- \tilde{r}}}{\lambda_-}\right], \tag{3.4a}$$

$$\chi_1^{(o)} = \frac{\sin^2\theta}{4}[\mathrm{e}^{-\lambda_+ \tilde{r}} + \mathrm{e}^{-\lambda_- \tilde{r}}], \tag{3.4b}$$

where we have defined

$$\lambda_\pm = (1 + \mathrm{i})\sqrt{\frac{\omega}{2} \pm \cos\theta}. \tag{3.5}$$

This expression can also be found in Busse (1968). Note that the condition $\omega > 2$ guarantees that the boundary layer solution does not diverge for any value of θ. Such a divergence, called critical latitude singularity, is known to be a source of inner shear layers as documented for the case of precession (see e.g. Hollerbach & Kerswell 1995).

A similar solution is obtained in the viscous layer near the inner sphere using the local variable $\hat{r} = (r-a)/\sqrt{E}$:

$$\psi_1^{(i)} = -\alpha \frac{\mathrm{i}a^2 \sin^2\theta}{4}\left[\frac{1-\mathrm{e}^{-\lambda_+\hat{r}}}{\lambda_+} - \frac{1-\mathrm{e}^{-\lambda_-\hat{r}}}{\lambda_-}\right], \tag{3.6a}$$

$$\chi_1^{(i)} = \alpha \frac{a^2 \sin^2\theta}{4}[\mathrm{e}^{-\lambda_+\hat{r}} + \mathrm{e}^{-\lambda_-\hat{r}}]. \tag{3.6b}$$

As $\hat{r}$ (respectively $\tilde{r}$) goes to infinity, $\chi_1^{(i)}$ (respectively $\chi^{(o)}$) goes to zero while $\psi_1^{(i)}$ (respectively $\psi^{(o)}$) goes to a non-zero constant. This part of the solution is responsible for a contribution in the bulk at the order $\varepsilon\sqrt{E}$, which corresponds to the Ekman pumping.

4. Mean zonal flow

4.1. *Flow asymptotic structure*

We now consider the nonlinear solution at order ε^2. This second-order correction is created by the nonlinear interaction of the first-order solution with itself. Note first that the nonlinear interaction of the solution in the bulk (the Ekman pumping) is expected to generate a correction at order $\varepsilon^2 E$. As we shall see, this order is actually smaller than the order of the mean flow correction that we will find in the limit $E \to 0$. The main contribution in the bulk will be found to come from the nonlinear interactions in the boundary layers and to be of the form

$$\psi_2 \sim \sqrt{E}\,\bar{\psi}_2(r,\theta), \tag{4.1a}$$

$$\chi_2 \sim \bar{\chi}_2(r,\theta), \tag{4.1b}$$

where $\bar{\psi}_2$ and $\bar{\chi}_2$ are both independent of time and E.

Equations (2.2) and (2.3) imply that $\bar{\psi}_2$ and $\bar{\chi}_2$ would satisfy in the bulk

$$\left(\cos\theta\frac{\partial}{\partial r} - \frac{\sin\theta}{r}\frac{\partial}{\partial\theta}\right)\bar{\psi}_2 = 0 \quad \text{and} \quad \left(\cos\theta\frac{\partial}{\partial r} - \frac{\sin\theta}{r}\frac{\partial}{\partial\theta}\right)\bar{\chi}_2 = 0, \tag{4.2}$$

which can be rewritten in cylindrical polar coordinates (ρ, ϕ, z) as

$$\frac{\partial\bar{\psi}_2}{\partial z} = 0 \quad \text{and} \quad \frac{\partial\bar{\chi}_2}{\partial z} = 0. \tag{4.3}$$

This means that, in the bulk, these two functions would be dependent only on the radial coordinate $\rho = r\sin\theta$ and could be written as

$$\bar{\psi}_2(r,\theta) = \Psi_2(\rho), \tag{4.4a}$$

$$\bar{\chi}_2(r,\theta) = \mathscr{X}_2(\rho). \tag{4.4b}$$

This property is nothing but a consequence of the Taylor–Proudman theorem.

In the next section, we calculate the functions $\Psi_2(\rho)$ and $\mathscr{X}_2(\rho)$ by performing a matched asymptotic analysis of the solutions in the boundary layers and in the bulk. The asymptotic structure of the problem is provided in figure 1. In addition to the boundary layers, the volume is split into two main regions I and II. Because one of the boundary layers disappears when we cross the cylinder tangent to the inner core, different approximations are obtained in regions I and II. We shall see that the functions are discontinuous across the boundary between regions I and II and that

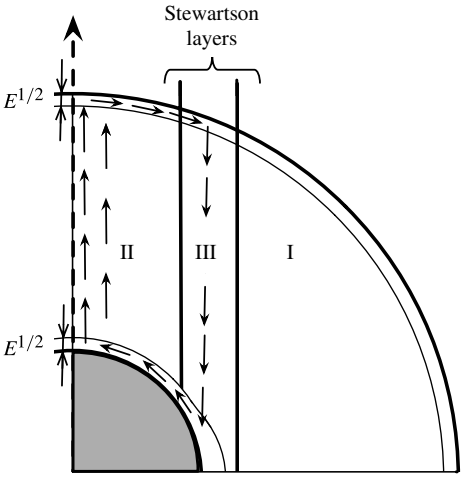

FIGURE 1. Structure of the flow in the librating shell, showing the presence of three different zones.

smoothing this singularity requires thin nested layers (region III) in which viscous effects have to be introduced.

In the following, we only consider mean flow quantities: the overbars are then dropped (e.g. $\bar{\chi}_2$ will be denoted χ_2).

4.2. *Boundary layer solution near the outer boundary* $r = 1$

Using the boundary layer variable $\tilde{r} = (1-r)/\sqrt{E}$, the equations (2.2) and (2.3) for the stationary component in the boundary layer at order ε^2 can be written

$$\frac{\partial^4 \psi_2^{(o)}}{\partial \tilde{r}^4} + 2\cos\theta \frac{\partial \chi_2^{(o)}}{\partial \tilde{r}} = NL_1^{(o)}, \tag{4.5}$$

$$\frac{\partial^2 \chi_2^{(o)}}{\partial \tilde{r}^2} - 2\cos\theta \frac{\partial \psi_2^{(o)}}{\partial \tilde{r}} = NL_2^{(o)}, \tag{4.6}$$

where $NL_1^{(o)}$ and $NL_2^{(o)}$ are the stationary part of the nonlinear forcing terms, given by

$$NL_1^{(o)} = -\frac{2\cos\theta}{\sin^2\theta}\left[\frac{\partial^2 \psi_1^{(o)}}{\partial \tilde{r}^2}\frac{\partial \psi_1^{(o)}}{\partial \tilde{r}} + \chi_1^{(o)}\frac{\partial \chi_1^{(o)}}{\partial \tilde{r}}\right] + \frac{1}{\sin\theta}\left[\frac{\partial \psi_1^{(o)}}{\partial \tilde{r}}\frac{\partial^3 \psi_1^{(o)}}{\partial\theta\,\partial \tilde{r}^2} - \frac{\partial \psi_1^{(o)}}{\partial\theta}\frac{\partial^3 \psi_1^{(o)}}{\partial \tilde{r}^3}\right], \tag{4.7}$$

$$NL_2^{(o)} = \frac{1}{\sin\theta}\left[\frac{\partial \psi_1^{(o)}}{\partial \tilde{r}}\frac{\partial \chi_1^{(o)}}{\partial\theta} - \frac{\partial \psi_1^{(o)}}{\partial\theta}\frac{\partial \chi_1^{(o)}}{\partial \tilde{r}}\right]. \tag{4.8}$$

From (4.5) and (4.6), we obtain a fifth-order equation for $\psi_2^{(o)}$:

$$\frac{\partial}{\partial \tilde{r}}\left[\frac{\partial^4}{\partial \tilde{r}^4} + 4\cos^2\theta\right]\psi_2^{(o)} = \frac{\partial NL_1^{(o)}}{\partial \tilde{r}} - 2\cos\theta\, NL_2^{(o)} = NL^{(o)}. \tag{4.9}$$

This equation has to be solved with the boundary conditions:

$$\psi_2^{(o)}(\tilde{r}=0)=0, \quad \frac{\partial \psi_2^{(o)}}{\partial \tilde{r}}(\tilde{r}=0)=0, \quad \lim_{\tilde{r}\to+\infty}\psi_2^{(o)}(\tilde{r})=\Psi_2(\sin\theta). \tag{4.10}$$

The expressions for $NL^{(o)}$ and $NL_1^{(o)}$ are cumbersome. We can write them in a compact form as

$$NL^{(o)}=\sum_{l=1}^{5}[A_l(\theta)+\tilde{r}B_l(\theta)]\mathrm{e}^{-\mu_l\tilde{r}}+\text{c.c.}, \tag{4.11a}$$

$$NL_1^{(o)}=\sum_{l=1}^{5}[C_l(\theta)+\tilde{r}D_l(\theta)]\mathrm{e}^{-\mu_l\tilde{r}}+\text{c.c.}, \tag{4.11b}$$

where the exponents μ_l are related to $\lambda_\pm$ defined in (3.5) by

$$\mu_1=\lambda_+ + \lambda_-^*, \quad \mu_2=\lambda_+ + \lambda_+^*, \quad \mu_3=\lambda_- + \lambda_-^*, \quad \mu_4=\lambda_+, \quad \mu_5=\lambda_-. \tag{4.12}$$

Expressions for the coefficients $A_l(\theta)$, $B_l(\theta)$, $C_l(\theta)$ and $D_l(\theta)$ are provided in appendix A.

The solution to (4.9) that satisfies the boundary conditions (4.10) reads

$$\psi_2^{(o)}(\tilde{r},\theta)=\phi_2^{(o)}(\tilde{r},\theta)+\Psi_2(\sin\theta)\left[1-\frac{\kappa^*\mathrm{e}^{-\kappa\tilde{r}}-\kappa\mathrm{e}^{-\kappa^*\tilde{r}}}{\kappa^*-\kappa}\right], \tag{4.13}$$

where

$$\begin{aligned}\phi_2^{(o)}(\tilde{r},\theta)=\sum_{l=1}^{5}\Bigg\{&-\frac{1}{4\cos^2\theta+{\mu_l}^4}\left[\frac{B_l+\mu_l A_l}{{\mu_l}^2}+\frac{4{\mu_l}^2 B_l}{4\cos^2\theta+{\mu_l}^4}\right]\\ &\times\left[\mathrm{e}^{-\mu_l\tilde{r}}+\frac{\mu_l-\kappa^*}{\kappa^*-\kappa}\mathrm{e}^{-\kappa\tilde{r}}+\frac{\mu_l-\kappa}{\kappa-\kappa^*}\mathrm{e}^{-\kappa^*\tilde{r}}\right]\\ &-\frac{B_l}{\mu_l(4\cos^2\theta+{\mu_l}^4)}\left[\tilde{r}\mathrm{e}^{-\mu_l\tilde{r}}-\frac{\mathrm{e}^{-\kappa\tilde{r}}-\mathrm{e}^{-\kappa^*\tilde{r}}}{\kappa^*-\kappa}\right]\Bigg\}+\text{c.c.},\end{aligned} \tag{4.14}$$

and where we have defined

$$\kappa=(1+\mathrm{i})\sqrt{\cos\theta}. \tag{4.15}$$

From (4.5), we obtain $\chi_2^{(o)}$, which must satisfy the matching condition

$$\lim_{\tilde{r}\to+\infty}\chi_2^{(o)}(\tilde{r})=\mathscr{X}_2(\sin\theta), \tag{4.16}$$

as

$$\begin{aligned}\chi_2^{(o)}(\tilde{r},\theta)=&\,\mathscr{X}_2(\sin\theta)\\ &-\frac{1}{2\cos\theta}\left[\frac{\partial^3\psi_2^{(o)}}{\partial\tilde{r}^3}+\left\{\sum_{l=1}^{5}\left(\frac{D_l+\mu_l C_l}{{\mu_l}^2}+\frac{\tilde{r}D_l}{\mu_l}\right)\mathrm{e}^{-\mu_l\tilde{r}}+\text{c.c.}\right\}\right].\end{aligned} \tag{4.17}$$

The above expression satisfies the no-slip boundary condition $\chi_2^{(o)}(0,\theta)=0$ only if Ψ_2 and $\mathscr{X}_2$ satisfies the relation

$$\mathscr{X}_2(\sin\theta)=\mathscr{F}(\sin\theta;\omega)-2\sqrt{\cos\theta}\,\Psi_2(\sin\theta), \tag{4.18}$$

where

$$\mathscr{F}(\sin\theta;\omega)=\frac{1}{2\cos\theta}\left[\left.\frac{\partial^3\phi_2^{(o)}}{\partial\tilde{r}^3}\right|_{\tilde{r}=0}+\left\{\sum_{l=1}^{5}\frac{D_l+\mu_l C_l}{{\mu_l}^2}+\text{c.c.}\right\}\right]. \tag{4.19}$$

Equation (4.18) is a constraint obtained from the matching between the solution in the bulk and the solution in the boundary layer on the outer sphere.

A similar constraint is expected from the boundary layer on the inner sphere. The same analysis in this boundary layer leads to

$$\mathscr{X}_2(a\sin\theta)=\alpha^2a^2\mathscr{F}(\sin\theta;\omega)+2\sqrt{\cos\theta}\,\Psi_2(a\sin\theta). \tag{4.20}$$

4.3. *Solution in the bulk*

Relations (4.18) and (4.20) permit us to obtain the functions Ψ_2 and $\mathscr{X}_2$ that characterize the mean flow correction at leading order in the bulk.

We first consider region I, defined by $\rho > a$ (see figure 1). In this region, the only contribution comes from the viscous layer close to the outer sphere. However, the flow in this region must satisfy a condition of symmetry on the equator: the axial flow should be antisymmetric with respect to the equator and therefore should vanish on the equator. Since it does not depend on the axial coordinate, this condition implies that it should vanish everywhere in region I. In other words,

$$\Psi_2(\rho)=0, \tag{4.21}$$

from which we deduce from (4.18) that for $\rho > a$ (i.e. in region I)

$$\mathscr{X}_2(\rho)=\mathscr{F}(\rho;\omega). \tag{4.22}$$

In region II, both the conditions of matching with the inner and outer boundary layers have to be considered. Replacing $\sin\theta$ by ρ in (4.18) and $a\sin\theta$ by ρ in (4.20) leads to

$$\mathscr{X}_2(\rho)=-2\left[1-\rho^2\right]^{1/4}\Psi_2(\rho)+\mathscr{F}(\rho;\omega), \tag{4.23a}$$

$$\mathscr{X}_2(\rho)=2\left[1-(\rho/a)^2\right]^{1/4}\Psi_2(\rho)+\alpha^2a^2\mathscr{F}(\rho/a;\omega), \tag{4.23b}$$

from which we deduce, for $\rho < a$ (in region II), that

$$\Psi_2(\rho)=\frac{\mathscr{F}(\rho;\omega)-\alpha^2a^2\mathscr{F}(\rho/a;\omega)}{2\left(1-\rho^2\right)^{1/4}+2\left[1-(\rho/a)^2\right]^{1/4}}, \tag{4.24a}$$

$$\mathscr{X}_2(\rho)=\frac{\alpha^2a^2\left(1-\rho^2\right)^{1/4}\mathscr{F}(\rho/a;\omega)+\left[1-(\rho/a)^2\right]^{1/4}\mathscr{F}(\rho;\omega)}{\left(1-\rho^2\right)^{1/4}+\left[1-(\rho/a)^2\right]^{1/4}}. \tag{4.24b}$$

Using (2.1), we can also calculate from Ψ_2 and $\mathscr{X}_2$ the mean azimuthal velocity u_{ϕ_2}, the mean axial velocity u_{z_2} and the mean axial vorticity ω_{z_2}, which satisfy in regions I and II

$$u_{\phi_2}=\frac{\mathscr{X}_2}{\rho},\quad u_{z_2}=\frac{\sqrt{E}}{\rho}\frac{\partial\Psi_2}{\partial\rho},\quad \omega_{z_2}=\frac{1}{\rho}\frac{\partial\mathscr{X}_2}{\partial\rho}. \tag{4.25}$$

Note that expressions (4.24*a*) and (4.24*b*) resemble the expressions obtained by Proudman (1956) for the flow between two spheres rotating at different speeds. The difference is in the numerator, which is now a more complicated function associated with the nonlinear interaction in the boundary layer of the flow generated by libration.

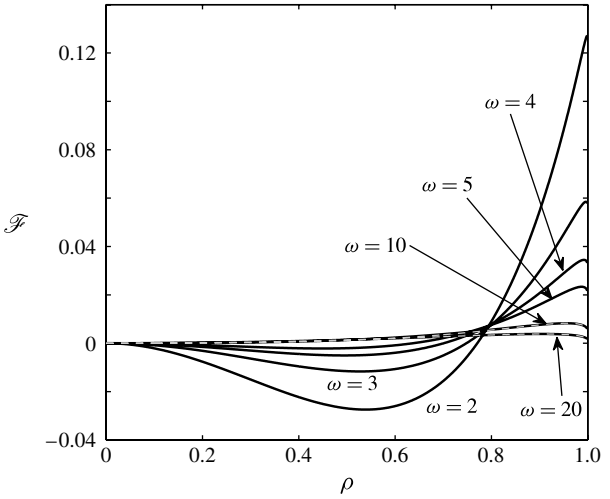

FIGURE 2. The function $\mathscr{F}(\rho;\omega)$ versus ρ for different values of the libration frequency ω. This function characterizes Ψ_2 and $\mathscr{X}_2$ in the bulk. Expression (4.27) is plotted in dashed grey for $\omega = 10$ and $\omega = 20$.

However, as in Proudman (1956), Ψ_2 and $\mathscr{X}_2$ exhibit a discontinuity across $\rho = a$. In particular, note that

$$\mathscr{X}_2(\rho) \underset{\rho\to a^+}{\sim} \mathscr{X}^+ = \mathscr{F}(a;\omega), \tag{4.26a}$$

$$\mathscr{X}_2(\rho) \underset{\rho\to a^-}{\sim} \mathscr{X}^- = \alpha^2 a^2 \mathscr{F}(1;\omega) = \frac{\alpha^2 a^2}{2\omega^2}. \tag{4.26b}$$

The singularities of Ψ_2 and $\mathscr{X}_2$ can be smoothed across a series of viscous layers as first shown by Stewartson (1966). In the next section, we provide approximations of the solution in these layers.

It is worth noting that the solution in region II can be deduced from the solution in region I. In other words, if we exclude the Stewartson layers, the solution in a spherical shell can be deduced from the solution in a sphere. Indeed, all the information is contained in the function $\mathscr{F}(\rho;\omega)$, which defines $\mathscr{X}_2$ in region I (or in a sphere). Unfortunately, we have not been able to obtain a simple expression for this function (see formula (B 1) given in appendix B). In figure 2, we have plotted $\mathscr{F}(\rho;\omega)$ versus ρ for various values of the libration frequency ω. A contour plot of $\mathscr{F}(\rho;\omega)$ in the (ρ,ω) plane is also shown in figure 3. Interestingly, we observe that $\mathscr{F}$ changes sign as ρ varies when $\omega < 8.5$. This means that the mean azimuthal flow generated by libration could be anticyclonic close to the axis and cyclonic further away.

For large libration frequency ω, an asymptotic expression for $\mathscr{F}(\rho;\omega)$ is obtained as

$$\mathscr{F}(\rho;\omega) \underset{\omega\to\infty}{\sim} \frac{\rho^2\sqrt{1-\rho^2}}{4\omega} - \frac{\sqrt{2}\rho^2\,(1-\rho^2)^{3/4}}{4\omega^{3/2}} + \frac{\rho^2(7\rho^2-5)}{4\omega^2} + o\left(\frac{1}{\omega^2}\right), \tag{4.27}$$

from which we can easily deduce the behaviour of $\mathscr{X}_2$, u_{ϕ_2}, Ψ_2 and u_{z_2}. In figure 2, we can observe that (4.27) provides a very good approximation for $\mathscr{F}$ for $\omega = 10$ and larger.

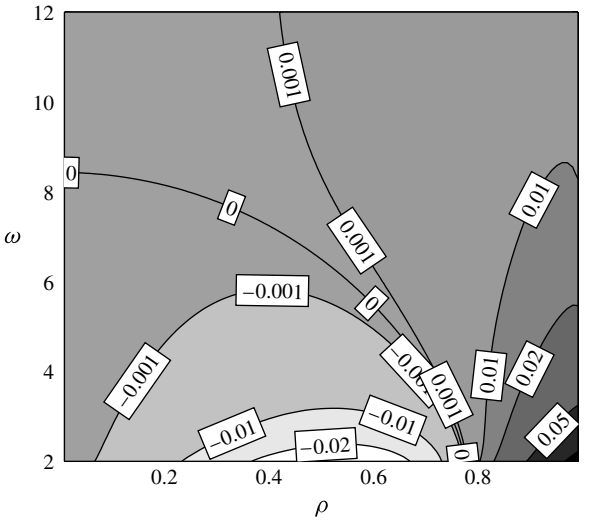

FIGURE 3. Contour levels of the function $\mathscr{F}(\rho;\omega)$ in the (ρ,ω) plane.

Close to $\rho=0$, the function $\mathscr{F}(\rho;\omega)$ can be related to the expression obtained for a cylinder (Wang 1970). We have $\mathscr{F}(\rho;\omega)\sim\Omega_{Cyl}(\omega)\rho^2$ as $\rho\to 0$, which leads to

$$\mathscr{X}_2 \underset{\rho\to 0}{\sim} \frac{(\alpha^2+1)}{2}\Omega_{Cyl}(\omega)\rho^2. \tag{4.28}$$

The function $\Omega_{Cyl}(\omega)$ corresponds to the mean angular velocity generated by the libration of a cylinder. Its expression was first obtained by Wang (1970) (see also Sauret *et al.* 2012). Note the simple expression for the function $\mathscr{F}$ at $\rho=1$: $\mathscr{F}(1;\omega)=1/(4\omega^2)$.

It is also interesting to provide expressions for Ψ_2 and $\mathscr{X}_2$ in the limit of a thin shell $(a\to 1)$:

$$\Psi_2 \sim (1-\alpha^2)\frac{\mathscr{F}(\rho;\omega)}{4\,(1-\rho^2)^{1/4}} + O(1-a), \tag{4.29a}$$

$$\mathscr{X}_2 \sim \frac{1+\alpha^2}{2}\mathscr{F}(\rho;\omega). \tag{4.29b}$$

Expression (4.29*a*) implies that Ψ_2 becomes small of order $(1-a)$ when the inner and outer spheres are librating at the same amplitude ($\alpha^2=1$). Expression (4.29*b*) means that the ρ dependence of the function $\mathscr{X}_2$ in the thin-shell limit is the same as for a full sphere.

4.4. *Solution in the Stewartson layers*

The structure of the viscous layers is the same as in Stewartson (1966) and is sketched in figure 4. There are three different layers around $\rho=a$: two outer layers scaling as $|\rho-a|=O(E^{1/4})$ for $\rho>a$, and $|\rho-a|=O(E^{2/7})$ for $\rho<a$, and an inner layer where $|\rho-a|=O(E^{1/3})$. As shown by Stewartson (1966), the outer layers guarantee the continuity of χ_2 (and u_{ϕ_2}) and of its first derivative, while the inner layer is for the smoothing of ψ_2 (and u_{z_2}) and higher derivatives of χ_2. More details on the calculation leading to approximations of the solution in each layer are given in appendix C. In this section, we only provide the leading approximation in each layer. In the appendix, we explain how the next order, which is $O(E^{1/28})$, can be obtained.

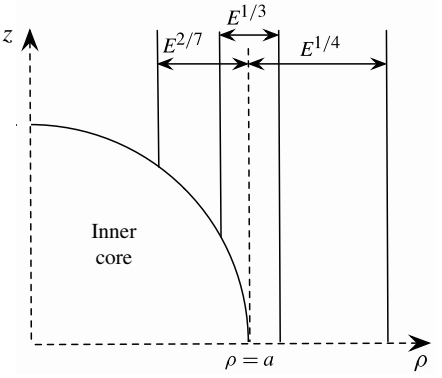

FIGURE 4. Structure of the Stewartson layers. The inner layer has a thickness of $E^{1/3}$, and the external and internal outer layers have a thickness of $E^{1/4}$ and $E^{2/7}$, respectively.

In the outer layers, simple expressions can be obtained. In the external outer layer ($\rho > a$), χ_2 varies exponentially between the two values $\mathscr{X}^{\pm} = \lim_{\rho \to a^{\pm}} \mathscr{X}_2(\rho)$ of $\mathscr{X}_2$ on either side of a in regions I and II:

$$\chi_2 \sim \mathscr{X}^{+}(1 - \mathrm{e}^{-\tilde{\rho}}) + \mathscr{X}^{-}\mathrm{e}^{-\tilde{\rho}}, \tag{4.30}$$

with

$$\tilde{\rho} = \frac{\rho - a}{(1 - a^2)^{3/8} E^{1/4}}. \tag{4.31}$$

In the internal outer layer ($\rho < a$), it is a constant:

$$\chi_2 \sim \mathscr{X}^{-}. \tag{4.32}$$

The function χ_2 (and therefore $u_{\phi 2}$) is thus of the same order in the Stewartson layers as in the bulk. By contrast, the vorticity associated with the mean flow correction is larger in the outer layers. Its main component is the axial component ω_{z_2}, which reads

$$\omega_{z_2} \sim E^{-1/4} \frac{\delta \mathscr{X}}{a\,(1 - a^2)^{3/8}} \mathrm{e}^{-\tilde{\rho}} \quad \text{in the external outer layer,} \tag{4.33a}$$

$$\omega_{z_2} \sim E^{-1/4} \frac{\delta \mathscr{X}}{a\,(1 - a^2)^{3/8}} \frac{\boldsymbol{f}'(\bar{\rho})}{\boldsymbol{f}'(0)} \quad \text{in the internal outer layer,} \tag{4.33b}$$

where the internal outer layer variable $\bar{\rho}$ is defined by

$$\bar{\rho} = (a - \rho)\left[\frac{a}{2E^2\,(1 - a^2)^2}\right]^{1/7}. \tag{4.34}$$

The function $\boldsymbol{f}$ is obtained in the appendix. It can be expressed in terms of Bessel functions (see expression (C 16)). In figure 5, we have plotted $\omega_{z_2}/\omega_{z_2}(a)$ in each outer layer. Note that the vorticity is strongly peaked at $\rho = a$, where it reaches its maximum value (in amplitude)

$$\omega_{z_2}(a) = E^{-1/4} \frac{\delta \mathscr{X}}{a\,(1 - a^2)^{3/8}}. \tag{4.35}$$

The discontinuity of the derivative at this point is smoothed in the inner layer.

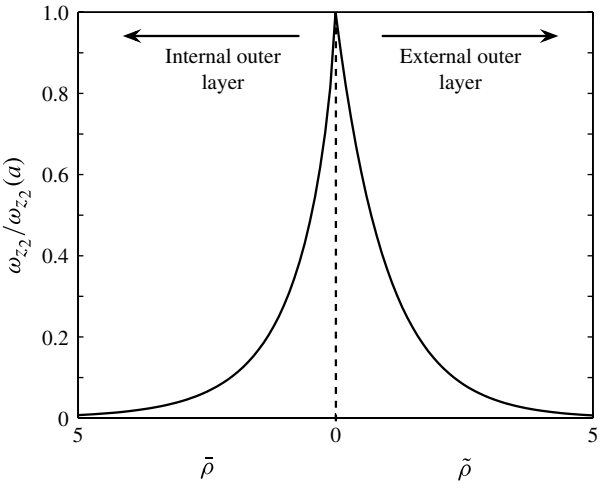

FIGURE 5. Axial vorticity $\omega_{z_2}/\omega_{z_2}(a)$ as a function of $\bar{\rho} = (a-\rho)\,[a/(2\,(1-a^2)^2\,E^2)]^{1/7}$ for $\rho < a$ (internal outer layer) and of $\tilde{\rho} = (\rho - a)/[(1-a^2)^{3/8}\,E^{1/4}]$ for $\rho > a$ (external outer layer).

Contrarily to the azimuthal velocity and the axial vorticity, the function ψ_2 and the axial velocity depend on the axial variable z at leading order. This dependence is linear in the outer layers (see expressions (C 8) and (C 18) in appendix C) but it is more complex in the inner layer. It is in this inner layer (where $|\rho - a| = O(E^{1/3})$) that ψ_2 and u_{z_2} are the largest. They scale respectively as $\psi_2 = O(E^{19/42})$ and $u_{z_2} = O(E^{5/42})$. Note, in particular, that the axial flow is much larger than in region II where it is $O(\sqrt{E})$. Unfortunately, the expressions for ψ_2 and u_{z_2} are not as simple as for χ_2. In the inner layer (where $|\rho - a| = O(E^{1/3})$), ψ_2 and u_{z_2} can be written as

$$\psi_2 \sim E^{19/42}\,\Lambda_3(a,\omega)\,\boldsymbol{I}\left(\frac{z}{\sqrt{1-a^2}},\frac{\rho-a}{E^{1/3}\,(1-a^2)^{1/6}}\right), \tag{4.36a}$$

$$u_{z_2} \sim E^{5/42}\,\Lambda_4(a,\omega)\,\boldsymbol{J}\left(\frac{z}{\sqrt{1-a^2}},\frac{\rho-a}{E^{1/3}\,(1-a^2)^{1/6}}\right), \tag{4.36b}$$

where $\boldsymbol{I}$ and $\boldsymbol{J}$ are the functions given in the appendix by (C 23) and (C 28), and Λ_3 and Λ_4 are related to $\delta\mathscr{X} = \mathscr{X}^+ - \mathscr{X}^- = \mathscr{F}(a;\omega) - \alpha^2 a^2/(4\omega^2)$ by

$$\Lambda_3(a,\omega) = \frac{\alpha_o a^{3/28}}{(1-a^2)^{11/84}}\delta\mathscr{X}(a,\omega), \tag{4.37a}$$

$$\Lambda_4(a,\omega) = \frac{\alpha_o}{a^{25/28}\,(1-a^2)^{25/84}}\delta\mathscr{X}(a,\omega), \tag{4.37b}$$

with $\alpha_o = -1/[2^{6/7}\boldsymbol{f}'(0)] \approx 0.45$.

The variations of the functions $\boldsymbol{I}(Z,R)$ and $\boldsymbol{J}(Z,R)$ with respect to R at various heights Z are shown in figure 6. Note that both functions are largest for small values of Z, that is, close to the inner sphere. It is also interesting to note the peculiar form of the axial flow profile, which is composed of a main jet surrounded by two weaker counter-propagating jets.

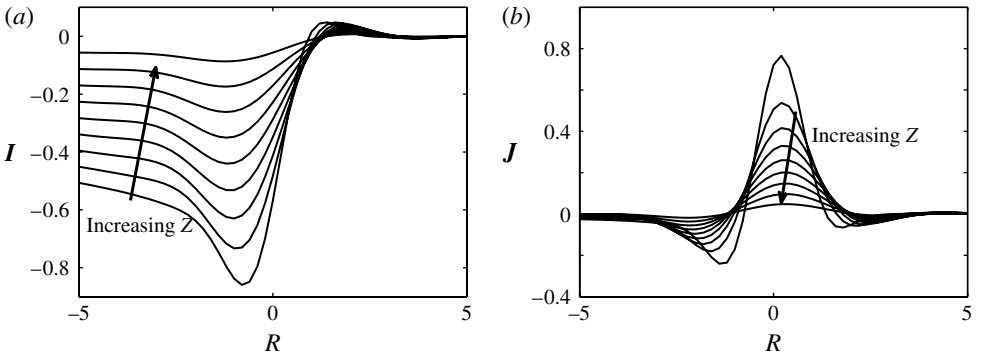

FIGURE 6. The functions (*a*) $\boldsymbol{I}(Z,R)$ and (*b*) $\boldsymbol{J}(Z,R)$ versus R for different values of Z ($Z=0.1$ to 0.9 in steps of 0.1). These two functions provide the spatial variation, in the inner layer, of ψ_2 and u_{z_2}, respectively.

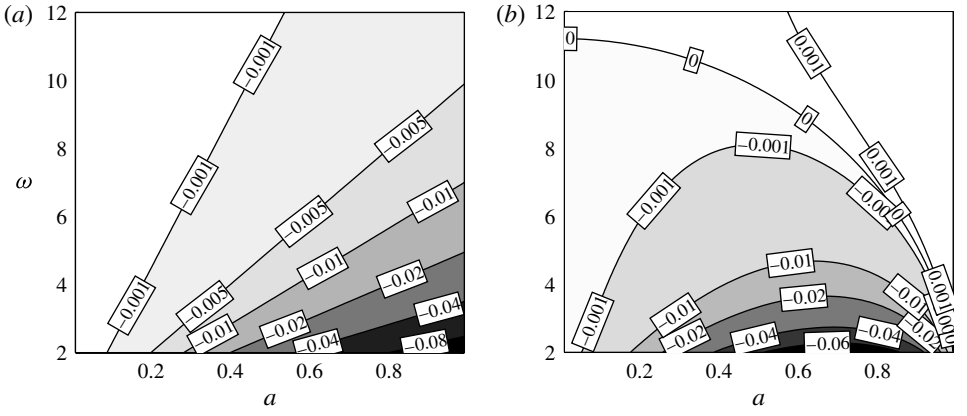

FIGURE 7. Contours of the function $\delta\mathscr{X}(a,\omega)$ in the (a,ω) plane. (*a*) When only the inner core is librating: $\delta\mathscr{X}(a,\omega)=-a^2/(4\omega^2)$. (*b*) When both spheres librate at the same amplitude ($\alpha=1$).

It is important to point out that ψ_2, u_{z_2} and ω_{z_2} depend on ω and α only via the function $\delta\mathscr{X}$ and that they are all proportional to that function. When the inner core is not librating, $\alpha=0$, and $\delta\mathscr{X}$ reduces to the function $\mathscr{F}(a;\omega)$, which has been plotted in figure 3. The libration of the inner sphere reduces the contribution from the outer sphere by a simple quantity $\alpha^2a^2/(4\omega^2)$. If only the inner core was librating (the outer sphere not librating) and if we had used for ε the amplitude of libration of the inner sphere, we would have obtained only the inner sphere contribution $\delta\mathscr{X}=-a^2/(4\omega^2)$. The contours of this function in the (a,ω) plane are plotted in figure 7(*a*). This plot, which describes the contribution from the inner sphere, has to be compared with the one obtained for the outer sphere contribution shown in figure 3. We clearly see that the contribution from the inner sphere is always of the same sign whatever a and ω: therefore, the libration of the inner core always generates a negative (anticyclonic) mean axial vorticity and a main axial flow that goes towards the inner sphere. In figure 7(*b*), we have plotted the variations of $\delta\mathscr{X}$ with respect to both variables a

and ω when the inner and outer spheres librate at the same amplitude ($\alpha = 1$). Note that, if we compare this plot with figure 3, we observe that the inner sphere provides a non-negligible contribution as soon as the radius a of the inner core is not small. In particular, it strongly increases the domain of parameters where the mean axial vorticity is anticyclonic.

5. Numerical comparison

In this section, the results of the asymptotic theory are compared to numerical results obtained for finite values of ε and E. Both published results obtained by Calkins *et al.* (2010) and results obtained using the finite elements commercial software Comsol Multiphysics are considered. Both codes rely on a two-dimensional (axisymmetric) model to be able to reach E values as small as $E = 10^{-6}$. For more details about our own numerical procedure, the reader is referred to Sauret *et al.* (2010, 2012) where the numerical procedure has already been used for similar problems.

The first and easiest comparison that can be made is for the libration in a sphere. In that case, there are no Stewartson layers and no axial flow in the bulk. The main contribution to the mean flow correction is an azimuthal flow, which is theoretically expected to be

$$u_\phi \sim \varepsilon^2 \frac{\mathscr{F}(\rho;\omega)}{\rho}, \tag{5.1}$$

for small Ekman number E and small libration amplitude ε.

Thus, the theory predicts that the zonal flow should scale as the square of the libration amplitude and be independent of the Ekman number. These properties have been tested by comparing numerical results obtained with Comsol Multiphysics to the theory for ε ranging from 0.01 to 0.3 and E ranging from 10^{-3} to 4×10^{-5}.

In figure 8(*a*), we display the results obtained for fixed frequency and amplitude and different Ekman numbers. We can observe that the numerical curve, which is already close to the theoretical curve for $E = 10^{-3}$, gets even closer as the Ekman number decreases. The departure obtained close to $\rho = 1$ is associated with the boundary layer on the outer sphere, which is not included in the theoretical expression (5.1) for the solution in the bulk. When E decreases, the boundary layer, which scales as $E^{1/2}$, becomes thinner, as observed. The amplitude ε has also been varied but its effect has been found to be very weak. For instance, the curves obtained for $\varepsilon = 0.01$ and $\varepsilon = 0.3$ cannot be distinguished from those plotted for $\varepsilon = 0.1$ in figure 8(*a*).

In figure 8(*b*), we have compared the theory to numerical results for different libration frequencies. Again, we observe a very good agreement for all frequencies. These results provide a validation of the asymptotic analysis that has led to expression (5.1).

In a librating shell, we expect from the theory that the azimuthal zonal flow remains independent of z in the bulk but exhibits a discontinuous behaviour across the cylinder tangent to the inner sphere at $\rho = a$. Such a discontinuity is visible in the numerical results. In figure 9(*a*), the numerical results obtained by Calkins *et al.* (2010) for two values of the Ekman number ($E = 10^{-5}$ and 10^{-6}) are compared with the theoretical prediction in the bulk (regions I and II).

The agreement is good if we do not consider the region close to $\rho = a = 0.35$, where the theoretical solution in the bulk is discontinuous. In particular, note that, for both Ekman numbers, and any value of z, the azimuthal velocity profiles collide far

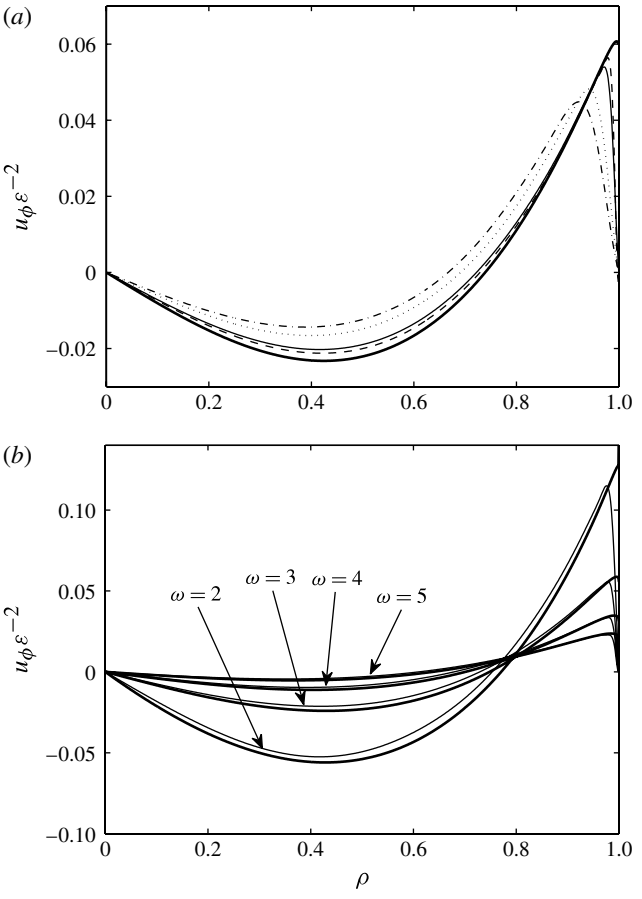

FIGURE 8. Mean azimuthal flow $u_{\phi_2} = u_\phi \varepsilon^{-2}$ in a sphere. Comparison of numerical results (thin lines) obtained in the equatorial plane ($z = 0$) with the theoretical results (thick lines). (*a*) For fixed frequency and amplitude (here $\omega = 3$, $\epsilon = 0.1$) and different Ekman numbers (dot-dashed line, $E = 10^{-3}$; dotted line, $E = 5 \times 10^{-4}$; (thin) solid line, $E = 10^{-4}$; dashed line, $E = 4 \times 10^{-5}$). (*b*) For fixed Ekman number and amplitude ($E = 5 \times 10^{-5}$, $\varepsilon = 0.01$) and different frequencies (as shown).

from $\rho = 0.35$ on a single curve, as expected from the theory. As in figure 8, the rapid localized variations observed in the numerical curves correspond to the boundary layer on the outer sphere $\rho^2 + z^2 = 1$. Their position changes because different z are considered. In the Stewartson layers, the solution becomes dependent on the Ekman number. In figure 9(*b*) the numerical results for $z = 0.6$ are plotted with respect to the outer layer variables $(\rho - a)/E^{1/4}$ and $(\rho - a)/E^{2/7}$. These results are compared to the leading-order theoretical prediction as well as to the second-order approximations obtained for $E = 10^{-6}$ in this plot. We can note first that there is a noticeable effect of the second-order correction on the theoretical curve. This correction, which is of the order of $E^{1/28}$, is clearly not small for an Ekman number $E = 10^{-6}$. If this correction is taken into account, a relatively good agreement is obtained between the theoretical curve and the numerical results close to $\rho = a$.

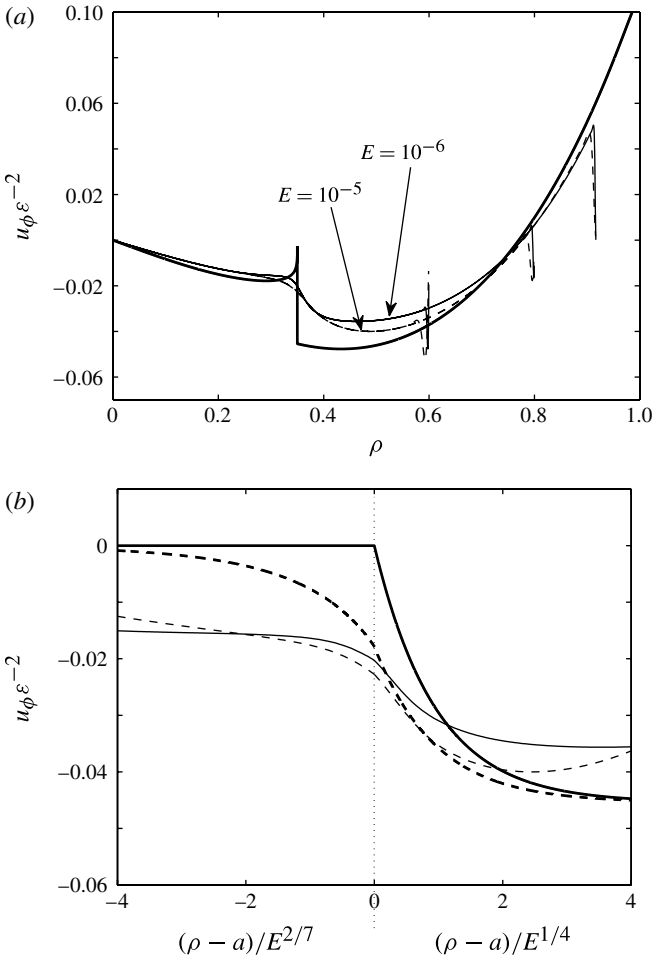

FIGURE 9. Mean azimuthal velocity for $\varepsilon = 2.2 \times 10^{-3}$, $a = 0.35$, $\omega = 2.2$ and $\alpha = 0$ (no libration of the inner core). (*a*) Solution in the bulk: $u_{\phi_2} = u_\phi \varepsilon^{-2}$ versus ρ. The thick solid line is the theoretical prediction in the bulk (regions I and II). The thin lines are the numerical results obtained by Calkins *et al.* (2010) at three different z ($z = 0.4,\ 0.6,\ 0.8$) and two different Ekman numbers ($E = 10^{-5}$, dashed line; $E = 10^{-6}$, solid line). (*b*) Solution in the Stewartson layers: $u_{\phi_2} = u_\phi \varepsilon^{-2}$ versus $(\rho - a)/E^{1/4}$ for $\rho > a$ and versus $(\rho - a)/E^{2/7}$ for $\rho < a$. The thick solid line is the leading-order theoretical prediction in the outer Stewartson layers. The thick dashed line is the theoretical prediction for $E = 10^{-6}$ where the correction in $E^{1/28}$ has been taken into account. The thin lines are the numerical results of Calkins *et al.* (2010) at $z = 0.6$ (solid line, $E = 10^{-6}$; dashed line, $E = 10^{-5}$).

A similar comparison is performed for the axial vorticity in figure 10 and for the axial velocity in figure 11. In figures 10(*a*) and 11(*a*), we have compared the numerical results with the theoretical solution in the bulk, that is (4.25) with (4.24*a*) and (4.24*b*) in region II ($r < a$), and with (4.21) and (4.22) in region I ($r > a$). A good agreement is observed far from $\rho = a$. Note, in particular, that both axial vorticity and axial velocity are independent of z far from a, as expected from the theory. However, there are systematic differences that were not present in the sphere. We suspect that these differences are due to $O(E^{1/28})$ corrections generated in the Stewartson layers,

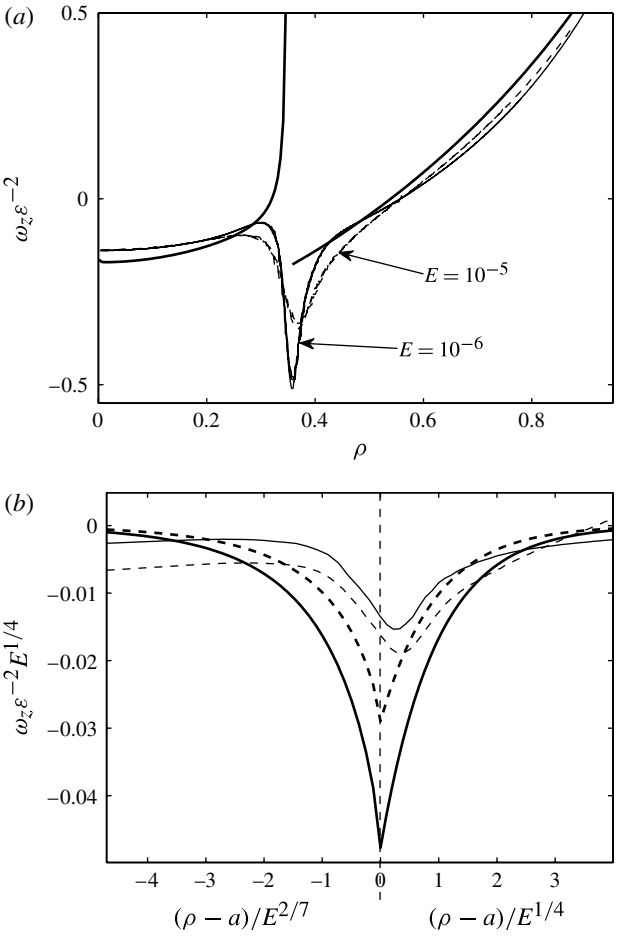

FIGURE 10. Mean axial vorticity for $\varepsilon = 2.2 \times 10^{-3}$, $a = 0.35$, $\omega = 2.2$ and $\alpha = 0$ (no libration of the inner core). (*a*) Solution in the bulk: $\omega_z\varepsilon^{-2}$ versus ρ. The thick solid line is the theoretical prediction in the bulk (regions I and II). The thin lines are the numerical results obtained by Calkins *et al.* (2010) at three different z ($z = 0.4,\ 0.6,\ 0.8$) and two different Ekman numbers ($E = 10^{-5}$, dashed line; $E = 10^{-6}$, solid line). (*b*) Solution in the Stewartson layers: $\omega_z\varepsilon^{-2}E^{1/4}$ versus $(\rho - a)/E^{1/4}$ for $\rho > a$ and versus $(\rho - a)/E^{2/7}$ for $\rho < a$. The thick solid line is the leading-order theoretical prediction in the outer Stewartson layers. The thick dashed line is the theoretical prediction for $E = 10^{-6}$ where the correction in $E^{1/28}$ has been taken into account. The thin lines are the numerical results of Calkins *et al.* (2010) at $z = 0.6$ (solid line, $E = 10^{-6}$; dashed line, $E = 10^{-5}$).

and which are not negligible for $E = 10^{-6}$. In figure 10(*b*), the axial vorticity is plotted with respect to the outer layer variables. Although a slight shift is observed in the numerical results, we can see that the vorticity peak with its scaling in $E^{-1/4}$ is qualitatively described. In figure 11(*b*), the axial velocity is plotted with respect to the inner layer variable. The agreement of the numerical results with the second-order theoretical approximation is remarkable for this value of z. Again, a slight shift is observed, which seems to diminish as E decreases. Other values of z have also been tested, and a less good agreement has been observed for smaller values of z. The numerical results shows a weaker jet, whereas the theory predicts the opposite. We

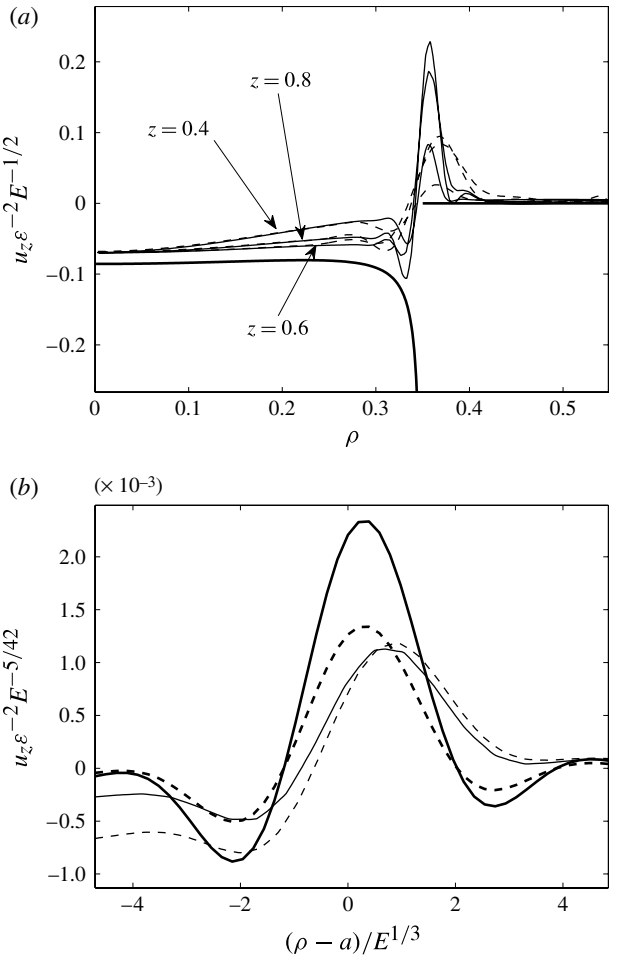

FIGURE 11. Mean axial velocity for $\varepsilon = 2.2 \times 10^{-3}$, $a = 0.35$, $\omega = 2.2$ and $\alpha = 0$ (no libration of the inner core). (*a*) Solution in the bulk: $u_z\varepsilon^{-2}E^{-1/2}$ versus ρ. The thick solid line is the theoretical prediction in the bulk (regions I and II). The thin lines are the numerical results obtained by Calkins *et al.* (2010) at three different z ($z = 0.4,\ 0.6,\ 0.8$) and two different Ekman numbers ($E = 10^{-5}$, dashed line; $E = 10^{-6}$, solid line). (*b*) Solution in the inner Stewartson layer at $z = 0.7$: $u_z\varepsilon^{-2}E^{-5/42}$ versus $(\rho - a)/E^{1/3}$. The thick solid line is the leading-order theoretical prediction in the inner Stewartson layer. The thick dashed line is the theoretical prediction for $E = 10^{-6}$ where the correction in $E^{1/28}$ has been taken into account. The thin lines are the numerical results of Calkins *et al.* (2010) at $z = 0.7$ (solid line, $E = 10^{-6}$; dashed line, $E = 10^{-5}$).

suspect that this qualitative difference could be due not only to the large value of the Ekman number but also to the particular structure of the Stewartson layer for small z, which has not been resolved here.

6. Conclusion

In this paper, we have analysed the mean flow induced by longitudinal libration (that is, small oscillation of the rotation rate) in a spherical shell and in a sphere, when

the oscillation frequency is larger than twice the mean rotation rate. Using asymptotic methods in the limit of small Ekman numbers E and small oscillation amplitude ε, we have been able to show that the main contribution to the mean flow is, in the bulk, an azimuthal flow that scales as ε^2, remains independent of the Ekman number and depends on the cylindrical variable ρ only. We have shown how such a zonal flow is generated by nonlinear interaction of the harmonic solution in the boundary layers. The dependence of the zonal flow with respect to the libration frequency ω and the ratio of the core size a has also been comprehensively analysed. In particular, we have shown how the zonal flow in a shell can be deduced from the zonal flow in a sphere. We have also seen that, for moderate frequencies $2 < \omega < 8.5$, both cyclonic and anticyclonic mean rotation can be created by libration, whereas only weak cyclonic rotation is created for $\omega > 8.5$.

The presence of the inner sphere has also been shown to create a discontinuity of the azimuthal flow across the tangent cylinder at $\rho = a$, which is smoothed in a series of nested viscous layers of widths $E^{1/4}$, $E^{2/7}$ and $E^{1/3}$, as for the configuration of differentially rotating spheres (Stewartson 1966). The mean flow correction has been calculated in each of these layers. We have obtained that an axial vorticity field of order $\varepsilon^2 E^{-1/4}$ is created in the outer Stewartson layers, and that a non-uniform axial flow of order $\varepsilon^2 E^{5/42}$ is present in the inner layer ($|\rho - a| = O(E^{1/3})$). We have shown that the spatial structures of these two fields in the Stewartson layers are universal functions that do not depend (after rescaling) on any parameter. The ratio of the core size, the oscillation frequency as well as the relative oscillation amplitude of the inner sphere, have been shown only to intervene in an amplitude factor, which has been fully characterized. In particular, we have demonstrated that the libration of the inner sphere adds a very simple quantity to the amplitude factor obtained without inner sphere libration, which always tends to increase the anticyclonicity of the vorticity field, and to add an axial flow from the inner core to the outer sphere.

The asymptotic results have been compared to numerical results in the literature (Calkins *et al.* 2010) or obtained with a finite-element code, and a good agreement has been demonstrated for the zonal flow in the bulk. A reasonable agreement has also been obtained for the peculiar structure of the solution in the Stewartson layers despite the largeness of the Ekman number in the simulations. In particular, we have shown that it was necessary to consider the second-order $O(E^{1/28})$ correction to obtain a correct agreement. It is worth mentioning that our theory is valid up to $O(E^{1/14})$. Even for realistic astrophysical values of E ($E \approx 10^{-14}$), we cannot guarantee that the error will remain small. This constitutes a weak point of the theory that is important to keep in mind when the results are applied.

7. Discussion

The present paper has considered oscillation frequencies larger than twice the rotation rate in a spherical shell. We can naturally address the question of the libration response when the frequency is smaller than twice the rotation rate or when the boundaries of the shell are elliptically deformed (that is, the outer and inner spheres are ellipsoids).

The first point has already been addressed in a cylinder (Wang 1970; Sauret *et al.* 2012) and for vanishingly small frequencies in a sphere (Busse 2010*a*; Sauret *et al.* 2010). For this point, the first difficulty comes from the fact that inertial modes can be resonantly excited by the harmonic forcing (Tilgner 2007; Morize *et al.* 2010). When this occurs, the zonal flow is strongly modified and is no longer dominated by the

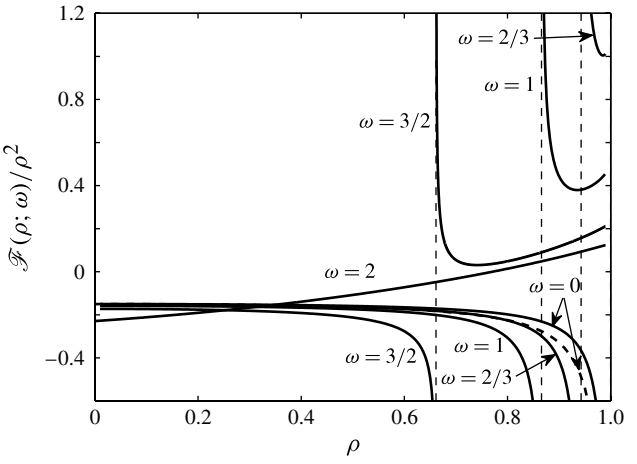

FIGURE 12. The function $\mathscr{F}(\rho;\omega)/\rho^2$ versus ρ for different values of ω between 0 and 2. The function $\mathscr{F}$ diverges at $\rho_c = \sqrt{1-\omega^2/4}$. Expressions (B 1) and (B 3) have been used for $\mathscr{F}$ for $\omega > 0$. The dashed line for $\omega = 0$ is the expression (7.2) obtained by Busse (2010*a*).

nonlinear interaction in the boundary layers (Sauret *et al.* 2012). The second difficulty is the singular behaviour of the boundary layer solution when twice the cosine of the inclination angle of the boundary matches the oscillation frequency. This singularity is known to generate internal shear layers in the bulk (see Kerswell 1995; Kida 2011), the effects of which on the mean flow remain to be quantified.

If we neglect the effect of such internal shear layers and assume no resonance, the mean zonal flow can be calculated using the same approach as for $\omega > 2$. The expressions (4.21), (4.22), (4.24*a*) and (4.24*b*) for Ψ_2 and $\mathscr{X}_2$ still apply, but expression (B 1) for $\mathscr{F}(\rho;\omega)$ obtained for $\omega > 2$ can only be used for $\rho > \rho_c = \sqrt{1-\omega^2/4}$. For $\rho < \rho_c$, expression (B 3) has to be used. This expression is obtained by the same analysis by changing the definition of the square root in (3.5). The two expressions diverge at ρ_c, which corresponds to the radius of the critical latitude on the outer sphere. In a shell, this singularity in $\mathscr{F}$ implies two singularities in $\mathscr{X}_2$. The second one, which is associated with the critical latitude on the inner sphere, is at $\rho_c = a\sqrt{1-\omega^2/4}$. From an asymptotic point of view, these singularities mean that another scaling has to be found for $\mathscr{X}_2$ close to each singularity.

In figure 12, we have plotted $\mathscr{F}/\rho^2$, that is, the angular velocity of the zonal flow in region I (see figure 1), for different values of ω. It is interesting to note that, for frequencies ranging from 0 to 1, we obtain almost the same constant retrograde rotation for all $\rho < 0.6$.

As $\omega \to 0$, expression (B 3) reduces to

$$\mathscr{F}(\rho;\omega) \sim \frac{(59\rho^2 - 72)\rho^2}{480(1-\rho^2)}. \tag{7.1}$$

This expression differs slightly from the expression obtained by Busse (2010*a*), which reads

$$\mathscr{F}(\rho;\omega) \sim \frac{(51.8\rho^2 - 72)\rho^2}{480(1-\rho^2)}. \tag{7.2}$$

Expression (7.1) is valid when $\varepsilon \ll \omega \ll 1$, whereas Busse's expression applies when $\omega \ll \varepsilon$. As noticed in figure 12, the difference between these two expressions is particularly visible for $\rho > 0.7$.

The low-frequency limit is interesting because low-frequency inertial modes are generally too damped to be resonantly excited. Moreover, for small ω, internal shear layers are limited to the very small region near the equator and to the neighbourhood of the cylinder tangent to the inner sphere, that is, within the Stewartson layers. Therefore, they are disconnected from the bulk regions I and II where our solution is expected to apply.

The second point, that is, the libration response in an ellipsoid, has also been addressed in the literature (Chan, Liao & Zhang 2011; Zhang, Chan & Liao 2011). When the ellipsoid is axisymmetric with respect to the rotation axis, our asymptotic analysis can be very easily adapted to find the zonal flow, which will not be fundamentally different from that in the sphere. By contrast, when the container is no longer axisymmetric along the rotation axis, the driving mechanism of the zonal flow may change, as it may no longer be associated with nonlinear interaction of boundary layer solution but with nonlinear interaction in the bulk of pressure forced solutions.

The two issues considered in this section are also discussed in the recent paper by Noir *et al.* (2012).

Acknowledgements

We would like to thank M. A. Calkins for having provided the numerical data published in Calkins *et al.* (2010) for the comparison done in § 5. This work has benefited from discussions with M. Le Bars, D. Cébron and F. Busse. We would also like to acknowledge discussions with N. Rambaux and C. Moutoux concerning the astrophysical applications of our results to Galilean satellites and exoplanetary systems.

Appendix A. The nonlinear coefficients A_l, B_l, C_l and D_l

The coefficients appearing in expressions (4.11*a*) and (4.11*b*) are given by

$$\begin{aligned} A_1 = \frac{\sin^2\theta}{16 {s_-}^3 {s_+}^3}[&4 {s_-}^2 (s_- + \mathrm{i}s_+)^2 {s_+}^2 \cos^2\theta \\ &+ (-{s_-}^6 + {s_-}^4 {s_+}^2 - 4\mathrm{i}{s_-}^3 {s_+}^3 - {s_-}^2 {s_+}^4 + {s_+}^6)\sin^2\theta \\ &+ \cos\theta(-4{s_-}^2 {s_+}^2 ({s_-}^2 + {s_+}^2)^2 + ({s_-}^4 + {s_+}^4)\sin^2\theta)], \end{aligned} \tag{A 1a}$$

$$B_1 = -\frac{(1-\mathrm{i})}{16 {s_-}^2 {s_+}^2}({s_-}^2 + {s_+}^2)(s_- + \mathrm{i}s_+)((s_- - \mathrm{i}s_+)^2 - \cos\theta)\sin^4\theta, \tag{A 1b}$$

$$A_2 = \frac{\sin^2\theta \cos\theta}{16 {s_+}^2}(4 {s_+}^2 \cos\theta + \sin^2\theta), \tag{A 1c}$$

$$A_3 = \frac{\sin^2\theta \cos\theta}{16 {s_-}^2}(-4 {s_-}^2 \cos\theta + \sin^2\theta), \tag{A 1d}$$

$$A_4 = -\frac{\sin^2\theta}{16 {s_-}^3 {s_+}^2}({s_+}^2 + \cos\theta)(4\cos\theta(s_- - s_+){s_+}^2 {s_-}^2 + \sin^2\theta({s_+}^3 + {s_-}^3)), \tag{A 1e}$$

$$A_5 = \frac{\sin^2\theta}{16{s_-}^2{s_+}^3}({s_-}^2 - \cos\theta)(4\cos\theta(s_- - s_+){s_+}^2{s_-}^2 + \sin^2\theta({s_+}^3 + {s_-}^3)), \quad (A\,1f)$$

$$B_2 = B_3 = B_4 = B_5 = 0, \quad (A\,1g)$$

$$C_1 = \frac{(1-\mathrm{i})\sin^2\theta}{32{s_-}^3{s_+}^3}[({s_-}^5 - {s_-}^3{s_+}^2 - \mathrm{i}{s_-}^2{s_+}^3 + \mathrm{i}{s_+}^5)\sin^2\theta$$
$$+ 4{s_-}^2(s_- - \mathrm{i}s_+)({s_-}^2 + {s_+}^2){s_+}^2\cos\theta], \quad (A\,1h)$$

$$D_1 = \frac{\mathrm{i}\sin^4\theta}{16{s_-}^2{s_+}^2}({s_+}^2 + {s_-}^2)^2, \quad (A\,1i)$$

$$C_4 = \frac{(1-\mathrm{i})\sin^2\theta}{32{s_-}^3 s_+}(4\cos\theta(s_- - s_+){s_+}^2{s_-}^2 + \sin^2\theta({s_+}^3 + {s_-}^3)), \quad (A\,1j)$$

$$C_5 = -\frac{(1-\mathrm{i})\sin^2\theta}{32{s_+}^3 s_-}(4\cos\theta(s_- - s_+){s_+}^2{s_-}^2 + \sin^2\theta({s_+}^3 + {s_-}^3)), \quad (A\,1k)$$

$$C_2 = D_2 = C_3 = D_3 = D_4 = D_5 = 0, \quad (A\,1l)$$

where

$$s_+ = \sqrt{\frac{\omega}{2} + \cos\theta}, \quad s_- = \sqrt{\frac{\omega}{2} - \cos\theta}. \quad (A\,2)$$

Appendix B. The function $\mathscr{F}(\rho;\omega)$

For $\omega > 2$, we have the following expression for $\mathscr{F}(\rho;\omega)$ with $\rho = \sin\theta$:

$$\begin{aligned}
\mathscr{F}(\sin\theta;\omega) = {} & \left[\frac{({s_+}^3 + {s_-}^3)\sin^4\theta}{32{s_+}^2{s_-}^2} + \frac{(s_- - s_+)\cos\theta\sin^2\theta}{8}\right] \\
& \times \left[\frac{s_+ - \sqrt{\cos\theta}}{{s_+}^2 + \cos\theta} - \frac{s_- - \sqrt{\cos\theta}}{{s_-}^2 - \cos\theta}\right] \\
& + \frac{\sin^2\theta(s_+ + \sqrt{\cos\theta})}{32{s_+}^3({\cos}^2\theta + 4{s_+}^4)}[2{s_+}^2 - 2s_+\sqrt{\cos\theta} + \cos\theta][\sin^2\theta + 4{s_+}^2\cos\theta] \\
& + \frac{\sin^2\theta(s_- + \sqrt{\cos\theta})}{32{s_-}^3({\cos}^2\theta + 4{s_-}^4)}[2{s_-}^2 - 2s_-\sqrt{\cos\theta} + \cos\theta][\sin^2\theta - 4{s_-}^2\cos\theta] \\
& - \frac{\sin^2\theta}{32{s_-}^3{s_+}^3({s_-}^2 + {s_+}^2)\,[{s_-}^2 + {s_+}^2 + 2s_+\sqrt{\cos\theta} + \cos\theta]^2} \\
& \times \big\{({s_-}^2 + {s_+}^2)[{s_-}^6 + 7{s_+}^2{s_-}^4 + 8{s_-}^7{s_+}^3 - 7{s_-}^2{s_+}^4 + 16{s_-}^5{s_+}^5 \\
& - {s_+}^6 + 4{s_+}^3{s_-}^3(-3 + 2{s_+}^4)] \\
& + [4{s_-}^6 s_+ - {s_-}^4{s_+}^3 - 16{s_-}^2{s_+}^5 - 3{s_+}^7 + 4{s_-}^5{s_+}^2(-3 + 16{s_+}^4) \\
& + {s_+}^4{s_-}^3(-19 + 32{s_+}^4) + {s_-}^7(-1 + 32{s_+}^4)]\sqrt{\cos\theta} \\
& + [4{s_-}^8{s_+}^2 - 3{s_+}^6 + {s_-}^6(1 - 20{s_+}^4) + {s_-}^2{s_+}^4(-11 + 4{s_+}^4) \\
& + 4{s_+}^3{s_-}^3(-3 + 16{s_+}^4) + {s_-}^5(-4s_+ + 64{s_+}^5) + {s_-}^4({s_+}^2 - 20{s_+}^6)]\cos\theta \\
& - [4{s_-}^7{s_+}^2 + 4{s_-}^6{s_+}^3 + {s_+}^5 + 56{s_-}^4{s_+}^5 + {s_-}^3{s_+}^2(3 - 76{s_+}^4) \\
& + {s_-}^5(1 - 8{s_+}^4) + 3{s_+}^3{s_-}^2(1 - 4{s_+}^4)]\cos^{3/2}\theta
\end{aligned}$$

$$
\begin{aligned}
&+[-{s_-}^8-4{s_-}^6{s_+}^2-4{s_+}^3{s_-}^5-48{s_-}^4{s_+}^4+60{s_+}^5{s_-}^3\\
&+20{s_-}^2{s_+}^6+{s_+}^8]\cos^2\theta\\
&+[{s_-}^7-4{s_-}^6s_++8{s_-}^5{s_+}^2-11{s_-}^4{s_+}^3+31{s_+}^4{s_-}^3\\
&+20{s_-}^2{s_+}^5+3{s_+}^7]\cos^{5/2}\\
&+[-{s_-}^6+4{s_-}^5s_+-{s_+}^2{s_-}^4+12{s_+}^3{s_-}^3+11{s_-}^2{s_+}^4+3{s_+}^6]\cos^3\theta\\
&+\ ({s_-}^5+3{s_-}^3{s_+}^2+3{s_+}^3{s_-}^2+{s_+}^5)\cos^{7/2}\theta\Big\}+\frac{\sin^2\theta}{4},
\end{aligned}
\tag{B 1}
$$

where

$$
s_+=\sqrt{\frac{\omega}{2}+\cos\theta}\quad\text{and}\quad s_-=\sqrt{\frac{\omega}{2}-\cos\theta}. \tag{B 2}
$$

For $\omega<2$, the above expression applies when $\rho>\rho_c=\sqrt{1-\omega^2/4}$. When $\rho<\rho_c$, we have to use the following expression with $\rho=\sin\theta$:

$$
\begin{aligned}
\mathscr{F}(\sin\theta;\omega)=\frac{\sin^2\theta}{32}\Bigg[&8+\frac{(l_++\sqrt{\cos\theta})(4{l_+}^2\cos\theta+\sin^2\theta)}{{l_+}^3(2{l_+}^2+2l_+\sqrt{\cos\theta}+\cos\theta)}\\
&+\frac{(l_-+\sqrt{\cos\theta})(4{l_-}^2\cos\theta+\sin^2\theta)}{{l_-}^3(2{l_-}^2+2l_-\sqrt{\cos\theta}+\cos\theta)}\\
&-\frac{4({l_-}^3+{l_-}^2\sqrt{\cos\theta}+(l_-+l_+)\cos\theta)}{l_+l_-(l_-+\sqrt{\cos\theta})}\\
&+\frac{{l_-}^4\sin^2\theta(l_-+\sqrt{\cos\theta}+({l_+}^3+{l_-}^3)/{l_-}^4\cos\theta)}{\cos\theta\,{l_+}^3{l_-}^3(l_-+\sqrt{\cos\theta})}\\
&-\frac{4({l_+}^3+{l_+}^2\sqrt{\cos\theta}+(l_++l_-)\cos\theta)}{l_-l_+(l_++\sqrt{\cos\theta})}\\
&+\frac{{l_+}^4\sin^2\theta(l_++\sqrt{\cos\theta}+({l_-}^3+{l_+}^3)/{l_+}^4\cos\theta)}{\cos\theta\,{l_-}^3{l_+}^3(l_++\sqrt{\cos\theta})}\\
&+\frac{1}{\cos\theta\,{l_-}^3{l_+}^3(l_-+l_+)\,(l_-+l_++\sqrt{\cos\theta})^2}\\
&\times\Big\{4{l_-}^2{l_+}^2(l_--l_+)^2\cos^{5/2}\theta[1+2(l_-+l_+)\sqrt{\cos\theta}]\\
&+\cos\theta[l_-l_+(l_-+l_+)(2(2{l_-}^2-3l_-l_++2{l_+}^2)\sin^2\theta\\
&+4{l_-}^5l_+-8{l_-}^3{l_+}^3+4l_-{l_+}^5)+2({l_-}^5+{l_+}^5)\sin^2\theta]\\
&+(l_-+l_+)^2({l_-}^4+{l_+}^4)\sin^2\theta[(l_-+l_+)+2\sqrt{\cos\theta}]\\
&+\cos^{3/2}\theta[8{l_+}^2{l_-}^2({l_-}^2-{l_+}^2)^2+({l_-}^4+{l_+}^4+l_-l_+(l_--l_+)^2)\sin^2\theta]\Big\}\Bigg]
\end{aligned}
\tag{B 3}
$$

where

$$
l_+=\sqrt{\cos\theta+\frac{\omega}{2}}\quad\text{and}\quad l_-=\sqrt{\cos\theta-\frac{\omega}{2}}. \tag{B 4}
$$

Appendix C. Stewartson layers

In this section, the solutions in the different layers around $\rho = a$ are provided. The analysis mainly follows the derivation given by Stewartson (1966). In all the layers, the functions ψ_2 and χ_2 are related at leading order in E by the same set of equations, which can be written in cylindrical coordinates as

$$2\frac{\partial \chi_2}{\partial z} = E\frac{\partial^4 \psi_2}{\partial \rho^4}, \tag{C 1a}$$

$$-2\frac{\partial \psi_2}{\partial z} = E\frac{\partial^2 \chi_2}{\partial \rho^2}. \tag{C 1b}$$

In the two outer layers (see figure 4), the function χ_2 remains at leading order in E independent of z, such that a simple relation between ψ_2 and χ_2 can be obtained by integrating (C 1*b*) with respect to z:

$$\psi_2(\rho, z) = -E\frac{z}{2}\frac{\partial^2 \chi_2}{\partial \rho^2} + B(\rho), \tag{C 2}$$

where $B(\rho)$ is a function to be determined in each outer layer.

External outer layer $E^{1/4}$

In the external outer layer of thickness $E^{1/4}$, the function ψ_2 must be antisymmetric with respect to the equator $z = 0$. This implies that $B(\rho) = 0$ in this layer. Another relation is obtained by considering the problem close to the boundary layer at $z = \sqrt{1-a^2}$. In this area, a relation between ψ_2 and χ_2 is deduced by writing (4.18) close to $\sin\theta = a$:

$$\chi_2(\rho) = -2\left(1-a^2\right)^{1/4} E^{-1/2}\psi_2(\rho, \sqrt{1-a^2}) + \mathscr{F}(a;\omega). \tag{C 3}$$

Evaluating (C 2) at $z = \sqrt{1-a^2}$ then leads to the equation

$$\frac{\partial^2 \chi_2}{\partial \rho^2} - \frac{\chi_2 - \mathscr{F}(a;\omega)}{E^{1/2}\left(1-a^2\right)^{3/4}} = 0, \tag{C 4}$$

which immediately gives

$$\chi_2(\rho) = \mathscr{F}(a;\omega) - \Lambda_1 \exp\left[-\frac{(\rho-a)E^{-1/4}}{\left(1-a^2\right)^{3/8}}\right]. \tag{C 5}$$

At this level, the constant Λ_1 is, *a priori*, unknown. We shall see below that it is given at leading order in E by

$$\Lambda_1 = \delta\mathscr{X} = \mathscr{X}^+ - \mathscr{X}^- = \mathscr{F}(a;\omega) - \frac{\alpha^2 a^2}{4\omega^2}. \tag{C 6}$$

In this layer, the axial vorticity is given by

$$\omega_{z_2} = \frac{1}{\rho}\frac{\partial \chi_2}{\partial \rho} = E^{-1/4}\frac{\delta\mathscr{X}(a,\omega)}{a\left(1-a^2\right)^{3/8}} \exp\left[-\frac{(\rho-a)E^{-1/4}}{\left(1-a^2\right)^{3/8}}\right], \tag{C 7}$$

while the function ψ_2 is given by the relation (C 2) with $B(\rho) = 0$:

$$\psi_2(\rho, z) = E^{1/2}\frac{z}{2}\frac{\delta\mathscr{X}(a,\omega)}{\left(1-a^2\right)^{3/4}} \exp\left[-\frac{(\rho-a)}{\left(1-a^2\right)^{3/8}E^{1/4}}\right]. \tag{C 8}$$

Internal outer layer $E^{2/7}$

The solution in the internal outer layer is obtained by considering the problem close to the two boundaries (at $z=0$ and $z=\sqrt{1-a^2}$). Close to the boundary on the inner sphere ($z=0$), we obtain a relation between ψ_2 and χ_2 by using (4.20):

$$\chi_2(\rho) = 2\left[1-(\rho/a)^2\right]^{1/4} E^{-1/2}\psi_2(\rho,0) + \frac{\alpha^2 a^2}{4\omega^2}. \tag{C 9}$$

Considering (C 2) at $z=0$, we then obtain $B(\rho)$ in this layer:

$$B(\rho) = \frac{\chi_2(\rho) - \alpha^2 a^2/(4\omega^2)}{2\left[1-(\rho/a)^2\right]^{1/4}}\sqrt{E}. \tag{C 10}$$

If we now use the relation (4.18), we obtain from (C 2), applied close to $z=\sqrt{1-a^2}$ with (C 10):

$$\frac{\partial^2\chi_2}{\partial\rho^2} - \frac{\chi_2 - \mathscr{F}(a)}{(1-a^2)^{3/4}\sqrt{E}} - \frac{\chi_2 - \alpha^2a^2/(4\omega^2)}{[2(a-\rho)]^{1/4}}\frac{a^{1/4}}{\sqrt{E}\sqrt{1-a^2}} = 0. \tag{C 11}$$

This equation leads to the solution

$$\chi_2(\rho) = \frac{\alpha^2a^2}{4\omega^2} + E^{1/28}\Lambda_2 \boldsymbol{f}(\bar{\rho}) + O(E^{1/14}), \tag{C 12}$$

with

$$\bar{\rho} = (a-\rho)\left[\frac{a}{2E^2\left(1-a^2\right)^2}\right]^{1/7} \tag{C 13}$$

and

$$\Lambda_2 = -\left(\frac{2}{a}\right)^{1/7}\frac{(1-a^2)^{-5/56}}{\boldsymbol{f}'(0)}\delta\mathscr{X}(a,\omega), \tag{C 14}$$

where the function $\boldsymbol{f}(s)$ satisfies

$$\frac{\partial^2\boldsymbol{f}}{\partial s^2} - \frac{\boldsymbol{f}}{s^{1/4}} = 0, \quad \boldsymbol{f}(0)=1, \quad \boldsymbol{f}(\infty)=0. \tag{C 15}$$

An explicit expression for $\boldsymbol{f}(s)$ is provided by

$$\boldsymbol{f}(s) = \frac{2\,(4/7)^{11/7}\,s^{1/2}\mathrm{K}_{4/7}(8/7s^{7/8})}{\Gamma(11/7)}, \tag{C 16}$$

where K_ν is the modified Bessel function of order ν and $\Gamma(z)$ is the Gamma function (Abramowitz & Stegun 1965). Note that $\boldsymbol{f}'(0) = -(4/7)^{8/7}\,\Gamma(3/7)/\Gamma(11/7) \approx -1.2246$.

The expressions (C 6) and (C 14) for Λ_1 and Λ_2 are such that χ_2 and $\partial_\rho\chi_2$, obtained from (C 3) and (C 9) for $\rho>a$ and $\rho<a$, respectively, are continuous at $\rho=a$. As shown by Stewartson (1966), this continuity condition comes from the condition of matching with the solution in the inner layer. It guarantees the continuity of the axial vorticity, which is given in the internal outer layer by

$$\omega_{z_2} = E^{-1/4}\frac{\Lambda_2}{2^{1/7}a^{6/7}\left(1-a^2\right)^{2/7}}\boldsymbol{f}'(\bar{\rho}). \tag{C 17}$$

Using (C 2) and (C 10)–(C 12), an expression for ψ_2 can be obtained:

$$\psi_2 \sim E^{13/28}\left(1-\frac{z}{\sqrt{1-a^2}}\right)\frac{\Lambda_2}{2^{9/7}a^{-2/7}\,(1-a^2)^{1/14}}\,\frac{\boldsymbol{f}(\bar{\rho})}{\bar{\rho}^{1/4}}. \tag{C 18}$$

Inner layer $E^{1/3}$

In the inner layer, χ_2 is constant and equal to $\alpha^2a^2/(4\omega^2)$. The function ψ_2 has by contrast a more complex structure. As shown by Stewartson (1966), $\psi_2 = O(E^{19/42})$ in the inner layer. More precisely, it can be written as

$$\psi_2 \sim E^{19/42}\Lambda_3(a,\omega)\,\boldsymbol{I}(R,Z), \tag{C 19}$$

with

$$R=\frac{(\rho-a)}{(1-a^2)^{1/6}\,E^{1/3}}, \tag{C 20a}$$

$$Z=\frac{z}{\sqrt{1-a^2}}, \tag{C 20b}$$

and $\boldsymbol{I}(R,Z)$ that satisfies

$$\frac{\partial^6\boldsymbol{I}}{\partial R^6}+4\frac{\partial^2\boldsymbol{I}}{\partial Z^2}=0, \tag{C 21}$$

with

$$(-2R)^{1/4}\boldsymbol{I}\sim 1 \quad \text{when } Z\to 0 \text{ for } R<0, \tag{C 22a}$$

$$(-2R)^{1/4}\boldsymbol{I}\sim (1-Z) \quad \text{when } R\to-\infty, \tag{C 22b}$$

$$\boldsymbol{I}(R,Z=1)=0, \tag{C 22c}$$

$$\boldsymbol{I}(R,Z=0)=0 \quad \text{for } R>0, \tag{C 22d}$$

$$\boldsymbol{I}\to 0 \quad \text{as } R\to+\infty. \tag{C 22e}$$

An integral form of $\boldsymbol{I}(R,Z)$ can easily be obtained from (C 21) using Fourier transform techniques as

$$\boldsymbol{I}(R,Z)=\frac{\Gamma(3/4)}{2^{1/4}\pi}\int_0^\infty \frac{\sinh[k^3(1-Z)/2]}{\sinh(k^3/2)}\,\frac{\cos(kR+3\pi/8)}{k^{3/4}}\,\mathrm{d}k. \tag{C 23}$$

The dependence of ψ_2 on ω is only in the function Λ_3, which is found to be

$$\Lambda_3(a,\omega)=-\frac{a^{3/28}}{2^{6/7}\boldsymbol{f}'(0)\,(1-a^2)^{11/84}}\delta\mathscr{X}(a,\omega). \tag{C 24}$$

The axial flow u_{z_2}, which can be deduced in the inner layer from ψ_2 by

$$u_{z_2}=\frac{1}{a}\frac{\partial\psi_2}{\partial\rho}, \tag{C 25}$$

is then given by

$$u_{z_2}\sim E^{5/12}\Lambda_4(a,\omega)\,\boldsymbol{J}(R,Z), \tag{C 26}$$

with

$$\Lambda_4(a,\omega)=\frac{\Lambda_3(a,\omega)}{a\,(1-a^2)^{1/6}}=-\frac{\delta\mathscr{X}(a,\omega)}{2^{6/7}\boldsymbol{f}'(0)a^{25/28}\,(1-a^2)^{25/84}} \tag{C 27}$$

and

$$\boldsymbol{J}(R,Z)=\frac{\Gamma(3/4)}{2^{1/4}\pi}\int_0^\infty \frac{\sinh[k^3(1-Z)/2]}{\sinh(k^3/2)}\cos(\pi/8-kR)k^{1/4}\,\mathrm{d}k. \tag{C 28}$$

For comparison with the numerical results, both leading-order and second-order approximations are used. Second-order approximations can be obtained by considering the $O(E^{1/28})$ correction to $\mathscr{X}^-$ deduced from (C 12):

$$\mathscr{X}^-=\frac{\alpha^2a^2}{4\omega^2}+E^{1/28}\Lambda_2\boldsymbol{f}(0). \tag{C 29}$$

This provides a new expression for $\delta\mathscr{X}$:

$$\delta\mathscr{X}=\frac{\mathscr{F}(a;\omega)-\alpha^2a^2/(4\omega^2)}{1+\zeta E^{1/28}}, \tag{C 30}$$

with

$$\zeta=-\left(\frac{2}{a}\right)^{1/7}(1-a^2)^{-5/56}\frac{\boldsymbol{f}(0)}{\boldsymbol{f}'(0)}. \tag{C 31}$$

If we use (C 30) in the expressions (C 6), (C 14), (C 24) and (C 27) for the coefficients Λ_1, Λ_2, Λ_3 and Λ_4, we obtain approximations valid up to $O(E^{1/14})$ corrections. It is these second-order approximations that have been used in figures 9(*b*), 10(*b*) and 11(*b*).

REFERENCES

Abramowitz, M. & Stegun, I. A. 1965 *Handbook of Mathematical Functions*. Dover.

Aldridge, K. D. 1967 An experimental study of axisymmetric inertial oscillations of a rotating liquid sphere. PhD thesis, Massachusetts Institute of Technology.

Aldridge, K. D. & Toomre, A. 1969 Axisymmetric inertial oscillations of a fluid in a rotating spherical container. *J. Fluid Mech.* **37**, 307–323.

Busse, F. H. 1968 Steady fluid flow in a precessing spheroidal shell. *J. Fluid Mech.* **33**, 739–751.

Busse, F. H. 2010*a* Mean zonal flows generated by librations of a rotating spherical cavity. *J. Fluid Mech.* **650**, 505–512.

Busse, F. H. 2010*b* Zonal flow induced by longitudinal librations of a rotating cylindrical cavity. *Physica* D **240**, 208–211.

Calkins, M. A., Noir, J., Eldredge, J. & Aurnou, J. M. 2010 Axisymmetric simulations of libration-driven fluid dynamics in a spherical shell geometry. *Phys. Fluids* **22**, 086602.

Chan, K. H., Liao, X. & Zhang, K. 2011 Simulations of fluid motion in ellipsoidal planetary cores driven by longitudinal libration. *Phys. Earth Planet. Inter.* **187**, 391–403.

Comstock, R. L. & Bills, B. G. 2003 A solar system survey of forced librations in longitude. *J. Geophys. Res.* **108**, 113.

Davis, S. H. 1976 The stability of time-periodic flows. *Annu. Rev. Fluid Mech.* **8**, 57–74.

Dormy, E. P. & Jault, D. 1998 MHD flow in a slightly differentially rotating spherical shell, with conducting inner core, in a dipolar magnetic field. *Earth Planet. Sci. Lett.* **160**, 15–30.

Ern, P. & Wesfreid, J. E. 1999 Flow between time-periodically co-rotating cylinders. *J. Fluid Mech.* **397**, 73–98.

Fischer, D. A., Marcy, G. W., Butler, R. P., Vogt, S. S., Laughlin, G., Henry, G. W., Abouav, D., Peek, K. M. G., Wright, J. T., Johnson, J. A., McCarthy, C. & Isaacson, H. 2008 Five planets orbiting 55 Cancri. *Astrophys. J.* **675**, 790–801.

Goldreich, P. & Peale, S. 1966 Spin–orbit coupling in the solar system. *Astron. J.* **397**, 73–98.

Hollerbach, R. & Kerswell, R. R. 1995 Oscillatory internal shear layers in rotating and precessing flows. *J. Fluid Mech.* **298**, 327–339.

KERSWELL, R. R. 1995 On the internal shear layers spawned by the critical regions in oscillatory Ekman boundary layers. *J. Fluid Mech.* **298**, 311–325.

KIDA, S. 2011 Steady flow in a rapidly rotating sphere with weak precession. *J. Fluid Mech.* **680**, 150–193.

LORENZ, R. D., STILES, B. W., KIRK, R. L., ALLISON, M. D., DEL MARMO, P. P., IESS, L., LUNINE, J. I., OSTRO, S. J. & HENSLEY, S. 2008 Titan's rotation reveals an internal ocean and changing zonal winds. *Science* **319** (5870), 1649–1651.

MARGOT, J. L., PEALE, S. J., JURGENS, R. F., SLADE, M. A. & HOLIN, I. V. 2007 Large amplitude libration of Mercury reveals a molten core. *Science* **316** (5825), 710–714.

MORIZE, C., LE BARS, M., LE GAL, P. & TILGNER, A. 2010 Experimental determination of zonal winds driven by tides. *Phys. Rev. Lett.* **104**, 214501.

NOIR, J., CALKINS, M. A., LASBLEIS, M., CANTWELL, J. & AURNOU, J. M. 2010 Experimental study of libration-driven zonal flows in a straight cylinder. *Phys. Earth Planet. Inter.* **182**, 98–106.

NOIR, J., CÉBRON, D., LE BARS, M., SAURET, A. & AURNOU, J. M. 2012 Experimental study of libration-driven zonal flows in non-axisymmetric containers. *Phys. Earth Planet. Inter.* **204–205**, 1–10.

NOIR, J., HEMMERLIN, F., WICHT, J., BACA, S. M. & AURNOU, J. M. 2009 An experimental and numerical study of librationally driven flow in planetary cores and subsurface oceans. *Phys. Earth Planet. Inter.* **173**, 141–152.

PROUDMAN, I. 1956 The almost-rigid rotation of viscous fluid between concentric spheres. *J. Fluid Mech.* **1**, 505–516.

RAMBAUX, N., VAN HOOLST, T. & KARATEKIN, Ö. 2011 Librational response of Europa, Ganymede, and Callisto with an ocean for non-Keplerian orbit. *Astron. Astrophys.* **527**, A118.

RIEUTORD, M. 1991 Linear theory of rotating fluids using spherical harmonics – II. Time-periodic flows. *Geophys. Astrophys. Fluid Dyn.* **59**, 185–208.

SAURET, A., CÉBRON, D., LE BARS, M. & LE DIZÈS, S. 2012 Fluid flows in a librating cylinder. *Phys. Fluids* **24**, 026603.

SAURET, A., CÉBRON, D., MORIZE, C. & LE BARS, M. 2010 Experimental and numerical study of mean zonal flows generated by librations of a rotating spherical cavity. *J. Fluid Mech.* **662**, 260–268.

SPOHN, T. & SCHUBERT, G. 2003 Oceans in the icy Galilean satellites of Jupiter? *Icarus* **161** (2), 456–467.

STEWARTSON, K. 1966 On almost rigid rotations. Part 2. *J. Fluid Mech.* **26**, 131–144.

SUESS, S. T. 1971 Viscous flow in a deformable rotating container. *J. Fluid Mech.* **45**, 189–201.

TILGNER, A. 1999 Driven inertial oscillations in spherical shells. *Phys. Rev.* E **59** (2), 1789–1794.

TILGNER, A. 2007 Zonal wind driven by inertial modes. *Phys. Rev. Lett.* **99**, 194501.

VAN HOOLST, T., RAMBAUX, N., KARATEKIN, Ö. , DEHANT, V. & RIVOLDINI, A. 2008 The librations, shape and icy shell of Europa. *Icarus* **195** (1), 386–399.

WANG, C. Y. 1970 Cylindrical tank of fluid oscillating about a steady rotation. *J. Fluid Mech.* **41**, 581–592.

WIECZOREK, M. A., CORREIA, A. C. M., LE FEUVRE, M., LASKAR, J. & RAMBAUX, N. 2012 Mercury's spin–orbit resonance explained by initial retrograde and subsequent synchronous rotation. *Nat. Geosci.* **5**, 18–21.

ZHANG, K., CHAN, K. H. & LIAO, X. 2011 On fluid motion in librating ellipsoids with moderate equatorial eccentricity. *J. Fluid Mech.* **673**, 468–479.